1-1-1980

Phyllosilicate fabric in naturally deformed mudstone from the Washington continental slope and comparison with experimentally induced fabric.

Peter L. Berglund

PHYLLOSILICATE FABRIC IN NATURALLY DEFORMED MUDSTONE FROM THE WASHINGTON CONTINENTAL SLOPE AND COMPARISON WITH EXPERIMENTALLY INDUCED FABRIC

by

Peter L. Berglund

A Thesis

Presented to the Graduate Comittee

of Lehigh University

in Candidacy for the Degree of

Master of Science

in

Geology

Lehigh University

1980

This thesis is accepted and approved in partial fulfillment of the requirements for the degree of Master of Science.

Sept. 20, 1980
(date)

Professor in Charge

Chairman of Department

ACKNOWLEDGEMENTS

Without the support, assistance, and advice from many people this thesis would not have been possible. I would like to thank: My wife Chris and children Carrie, Tim, and Brian, for suffering through my years as a student; Dr. Bobb Carson, for serving as my thesis advisor and for hiring me as a research assistant; Dr. Paul B. Myers, for serving on my thesis committee; Drs. Jan and Terry Tullis of Brown University Department of Geological Sciences, for allowing me the run of their x-ray lab; Dr Don Forsythe of that same department, for aid in the initial reduction of x-ray data; Dr. James Parks of Lehigh, for help in debugging my computer programs; and finally the National Science Foundation, whose funding (Grant OCE 76 21529) made possible the basic research, computer time, and other associated costs of this research project.

TABLE OF CONTENTS

LIST OF TABLES

LIST OF FIGURES

LIST OF PLATES

ABSTRACT

Convergent motion of the North American and Juan de Fuca plates has resulted in deformation of Cascadia Basin sediments and accretion of these deposits to the Washington-Oregon (lower) continental slope. Near-surface accreted deposits consist largely of Pleistocene/Pliocene mudstones, which have undergone mechanical consolidation.

Some of these deposits exhibit a rudimentary spaced cleavage. The foliation is inclined approximately 80° to bedding. Individual folia are typically spaced 1.5 to 2.0 mm apart, although the spacing varies from 0.5 to 10 mm. Observation by scanning electron and optical microscopy reveal the folia to be zones of subparallel phyllosilicate (clay) flakes. These zones range in width from 10 μm to 150 μm, are at least 10 cm long, and commonly anastomose. Along the edges of the folia, grains with an orientation intermediate between bedding and foliation are observed.

Disaggregated deep sea mudstone artificially deformed (total strain = -0.17; strain rate = 1.1×10^{-7} s^{-1}) in the laboratory also exhibits water loss (initial water content ~90 percent dry weight, final water content ~60 to 87 percent). The fabric resulting

from deformation, however, differs markedly from that of the natural mudstones. Two types of microstructures, shear fractures and crenulations, predominate. The former commonly dip 25° to 35° and range in length from 200 μm to 10 cm; in width, they vary from 15 to 20 μm to as much as 1 mm. The crenulations consist of lenticular domains, generally normal to the axis of maximum compressive strain, ranging in width from 20 to 300 μm, and in length up to 5 mm. Clay flakes are subparallel within the crenulations, with orientations alternating from domain to domain in a chevron pattern, with internal angles of 60° to 100°.

Preferred orientations in the artificially deformed mudstone measured by x-ray pole figure goniometry range from a maximum of 2.9 (in multiples of a random distribution) to 1.5; the directions of these preferred orientations vary widely from sample to sample, indicating a severe inhomogeneity of strain.

Although there are differences in fabric, there appear to be similarities in styles of deformation between the naturally and artificially deformed mudstones, and in both cases the resultant fabric appears to be intimately related with dewatering. In the natural mudstones, it appears that pore pressure, in response to tectonic overpressures, eventually exceeds lithostatic pressure, causing trapped pore fluids to migrate

along planes normal to the direction of shortening; these rapidly escaping fluids cause realignment of clay flakes, resulting in the spaced cleavage observed.

In the artificially deformed mud, water loss is uniform rather than rapid, perhaps due to a much lower lithostatic pressure. As clay flakes near the locus of deformation rotate into parallelism, water escapes between them. With increasing water loss and strain hardening, overthrusting occurs, and additional water then apparently escapes along shear planes.

While it is doubtful that tectonic dewatering is solely responsible for the formation of slaty cleavage, it is believed to be instrumental in formation of initial preferred orientations which are then modified and enhanced by further tectonic processes.

INTRODUCTION

The mechanisms responsible for development of secondary preferred phyllosilicate orientations in lutites may be related to the origins(s) of slaty cleavage. Slaty cleavage is defined as

> ... a planar fabric that is uniformly developed (or penetrative) throughout all the rock material

(Ramsay, 1967, p 177). Since virtually all slates contain significant percentages of phyllosilicates, this definition implies a strongly developed preferred orientation of platy or elongate mineral grains. This preferred orientation may be dimensional in the case of mineral constituents such as quartz, but is both dimensional and crystallographic in the case of phyllosilicates (Tullis, 1971). The pervasiveness of the fabric may vary (in intensity) with the degree of strain (Ramsay and Wood, 1973), and some slates are seen to consist of alternating domains of quartzofeldspathic material and phyllosilicates (Braddock, 1970; Williams, 1972; Geiser, 1974; Groshong, 1976). Slaty cleavage may show a gradational relationship with other types of rock cleavage, such as fracture and crenulation cleavage (Carson, W., 1968; Williams, 1972; Siddans, 1977), and with schistosity in coarser and more highly metamorphosed rocks (Moench, 1966).

The development of slaty cleavage is intimately associated with folding; its axial planar relationship was recognized early in the nineteenth century (Siddans, 1972). Numerous studies have shown that slaty cleavage develops normal to the maximum finite shortening, in the XY plane of the deformation ellipsoid (Cloos, 1947; Oertel, 1970; Tullis and Wood, 1975; Siddans, 1977). Experimentally produced preferred orientations of phyllosilicates have also confirmed this relationship (Means and Patterson, 1966; Quigley and Thompson, 1966; Clark, 1970b; Tullis, 1971; Chawla, 1973; Maltman, 1977). The strains determined from deformed objects in slates are quite large: Ramsay and Wood (1973) have found the dimensions of the mean strain ellipsoid for some 990 determinations to be 1.6 / 1 / 0.25, corresponding to 120 percent extension on X, 35 percent extension on Y, and 65 percent shortening on Z (X, Y, and Z being the principal axes of the finite strain ellipsoid). Similarly, Wood (1974) found the mean strain ellipsoid for over 5000 determinations to be 1.76 / 1 / 0.24. Geiser (1974), on the other hand, reports incipient cleavage zones in a silty mudstone which shows only six percent maximum shortening. All slates lie in the deformation field of apparent flattening (Ramsay and Wood, 1973).

Some authors have expressed alternate views on the perpendicularity of slaty cleavage to maximum finite

shortening. Williams (1976) states that slaty cleavage will parallel the XY plane only if the strain history is coaxial, which is not generally the case in folding. Furthermore, shear strain is actually observed on or parallel to some foliation surfaces, indicating that cleavage may develop on a plane of shear strain, although not necessarily that of maximum shear strain (Williams, 1976). Maxwell (1976) and Powell (1974) express the view that while slaty cleavage and folding are responses to the same compressive stress, they are not strictly contemporaneous events, with cleavage usually developing prior to, or early during, folding. Once formed, cleavage planes become strain markers subject to reorientation by subsequent deformation. Since

> ... texture producing processes that effect phyllosilicates are ... controlled by local stresses operating on the scale of strain increments,

(Siddans, 1976, p 52), there is no reason to expect rigid parallelism of cleavage with the XY plane of the bulk finite strain ellipsoid.

Concomitant with the development of a preferred orientation in phyllosilicates is a reduction in sediment volume. Ramsay and Wood (1973) estimate a volume decrease of 10 to 20 percent in development of slate from lithified mudstone, although they allow that some slates may develop under plane strain conditions with no volume loss. Maxwell (1962) estimates a volume loss of as much as 40 percent

in the transition from water saturated argillaceous sediments to slate.

It is clear that slaty cleavage is a plastic flow phenomenon. What has remained unclear, through nearly 150 years of field and experimental research, is the mechanism of phyllosilicate alignment within (parallel to) flow planes. The two mechanisms favored currently are: 1) mechanical rotation during tectonic dewatering (Maxwell, 1962; Moench, 1966, 1970; Carson, W., 1968; Powell, 1969, 1972a, 1972b, 1973, 1974; Braddock, 1970; Clark, 1970a; Alterman, 1973; Moore, 1973); and 2) pressure solution (solution transfer) (Durney, 1972; Williams, 1972; Boulter, 1974; Burger, 1974; Wood, 1974; Geiser, 1975; Holeywell and Tullis, 1975; Groshong, 1975, 1976; Siddans, 1977). These mechanisms differ not only in the proposed state of lithification at which slaty cleavage develops, but also in the suggested causes for the plasticity necessary for flowage to occur. According to the tectonic dewatering hypothesis, phyllosilicates are rotated in soft sediments made plastic by abnormally high pore pressures. According to the pressure solution hypothesis, platy mineral residues are left by the differential solution and recrystallization of soluble quartzofeldspathic material, plasticity being the result of elevated temperature and pressure. Preferred orientations developed by either mechanism can be enhanced by later,

syn- to post-tectonic recrystallization under metamorphic conditions (Oertel, 1970).

Maxwell's (1962) dewatering hypothesis is founded in part on the work of Ruby and Hubbert (1959; see also Hubbert and Ruby, 1959), who suggested that, under proper conditions, pore fluids may become trapped in buried sediments and attain anomalous pressures (pressures in excess of hydrostatic pressure) even approaching that of lithopressure. When this occurs, compaction of the sediments is prevented, and normal grain to grain pressures are largely supported by the pore fluid; thus the rotation of platy minerals under tectonic stress is facilitated. The conditions necessary for development of such high pore pressures are commonly taken to be rapid deposition and burial of interbedded argillaceous and arenaceous sediments (which act as fluid reservoirs), large total thickness, and rapid loading (Ruby and Hubbert, 1959). This loading can be either sedimentary or tectonic, but would necessarily be tectonic for the development of slaty cleavage. As parallelism of phyllosilicates increases, the developing anisotropic fabric increases permeability and dewatering occurs along cleavage planes (Alterman, 1973), allowing growth of new crystals of clays and chlorite (Moench, 1966).

The most frequently cited evidence for a soft sediment origin of slaty cleavage is the parallelism of

clastic dikes with cleavage (Maxwell, 1962; Moench, 1966, 1970; Powell, 1969, 1972a, 1972b, 1973; Braddock, 1970; Alterman, 1973; Moore, 1973). These dikes are presumably implaced by water-saturated sediment injections (Maxwell, 1976) which emanate from argillaceous or arenaceous beds when pore pressure exceeds confining pressure. Cleavage appears to be enhanced in the vicinity of the argillite injections (Clark, 1970a; Maxwell, 1976). Powell (1969, 1972a) sees the occurence of these "anastamosing pelitic folia" as an actual mechanism for development of preferred orientation; i.e., the escape of water causes alignment rather than the converse. It is notable that what appear to be the same type of pelitic folia are observed in mudstones from depths of 300 to 800 m in cores taken on DSDP Leg 57 in the vicinity of the Japan Trench (Carson, 1978, personal communication).

Proponents of a solid state origin for slaty cleavage explain dike-cleavage parallelism as being due to rotation of the dikes by large finite strain. (The development of parallelism by rotation with increasing strain is treated in Ramsay, 1967, 1976). Groshong (1976) calculated sufficient strain in the Martinsburg (-63 percent) to rotate dikes into parallelism; in addition, he cited numerous examples of clastic dikes in rocks possessing no cleavage, showing that no causal relationship exists between clastic dikes and cleavage. Boulter (1974)

graphically strained (-60 percent homogeneous plane strain) drawings of clastic dikes from uncleaved rocks, acheiving results similar in appearence to dikes found accompanied by cleavage. Geiser (1975) shows dikes that are extended (boudinage) when nearly parallel to cleavage, and folded when at high angles to cleavage. Furthermore, he states that parallelism of dikes to cleavage has not been conclusively demonstrated, with his own measurements from the Normanskill formation showing a mean dihedral dike-cleavage angle of 14 degrees.

These arguments are countered by Powell (1976), who found that when the direction of rotation is accounted for, his measurements from the Siamo slate how a dike-cleavage divergence of less than two degrees, small enough to allow statistical parallelism. Powell (1972a), Alterman (1976), and Maxwell (1976) all point out that the intrusion of clastic dikes is a brief event during deformation, and once formed, dikes may be rotated, possibly at a rate differing from that of individual phyllosilicate grains (Alterman, 1976).

A further objection to the dewatering hypothesis arises from the presence of deformed fossils in some slates (Wood, 1974). Fossils presumably deform contemporaneously with the matrix in which they lie, and thus their deformation in soft sediment is difficult to explain. Many slates, however, originate in black shale

environments, where reducing conditions might allow leaching of shells, making them as plastic as the surrounding sediment (Maxwell, 1976).

The solution transfer mechanism responsible for solid state development of slaty cleavage is elegantly explained in terms of nonhydrostatic thermodynamics by Durney (1972). Since solubility is a function of normal stress σ, mineral grains will dissolve along surfaces statistically normal to σ_1 (maximum compression axis) and will grow on surfaces normal to σ_3 (minimum compression axis). Dissolved material is transferred along grain boundaries by diffusion. These processes

> ... can occur under differential stresses lower than those required for most other rock deformation mechanisms...

(Durney, 1972, p 315). Up to 20 to 30 percent of the rock mass can be transferred in this manner (Burger, 1974). As volume and mechanical support are reduced with the removal of soluble mineral grains, the phyllosilicate residue becomes strongly aligned parallel to the pressure solution surface (Durney, 1972).

The pelitic folia which Powell (1969, 1972a) sees as dewatering phenomena are interpreted by others as insoluble residue left by selective pressure solution and transfer of quartzofeldspathic material (Williams, 1972; Geiser, 1975; Groshong, 1976). These folia are often separated by quartz-rich domains, in which grains

show pressure shadows and are truncated on their contacts with the pelitic domains (Groshong, 1976). The intensity of the slaty cleavage is a function of the relative quantities of these phyllosilicate and quartzofeldspathic domains (Williams, 1972).

From the preceeding discussion it is evident that the same field and petrographic evidence is often called upon in support of either mechanism of slaty cleavage development. This is due to the fact that virtually all of the rocks in which slaty cleavage has been studied have been subjected to at least low-grade metamorphism. Recrystallization and pressure solution can mask the effects of grain rotation during dewatering, rendering evidence inconclusive. While experimental studies (Means and Patterson, 1966; Clark, 1970b; Tullis, 1971; Chawla, 1973; Maltman, 1977) have shown mechanical rotation alone to be sufficient for the development of preferred orientation, in only two cases known to this author have (developing) preferred orientations been reported in deformed, but unlithified, Pleistocene sediments (Moore and Geigle, 1974; Barnes and Ross, 1975).

STATEMENT OF THE PROBLEM

It is the purpose of this study to determine if preferred orientations of phyllosilicates exist in tectonically deformed but unlithified (Pleistocene) mudstones

from the Washington continental margin, and to evaluate development of incipient slaty cleavage by deformation in this convergent tectonic setting. These preferred orientations will, furthermore, be described, characterized, and compared to preferred orientations artificially induced in the same sediment by laboratory experiment.

SEDIMENT SAMPLES AND GEOLOGIC SETTING.

The sediments used in this study are deformed mudstones dredged from the lower continental slope off Washington and northern Oregon (Carson, 1977). While these sediments are not lithified, they are sufficiently consolidated to allow dredging of coherent blocks which yield undisturbed, interior samples. In addition, disaggregated mud from one of the dredge samples has been artificially deformed in a squeezebox by horizontal compression under saturated but unconfined conditions (Carson, 1976). The sampling sites (fig. 1) lie on the westward (seaward) flanks of a series of imbricately thrusted anticlines which strike north-northwest/south-shoutheast along the lower Washington-Oregon continental slope (Carson et al, 1974; Carson, 1977). These folds are apparently the result of progressive accretion of offscraped Cascadia Basin sediments as the Gorda-Juan de Fuca plate subducts beneath the North American plate (Silver, 1972; von Huene and Kulm, 1973; Carson et al,

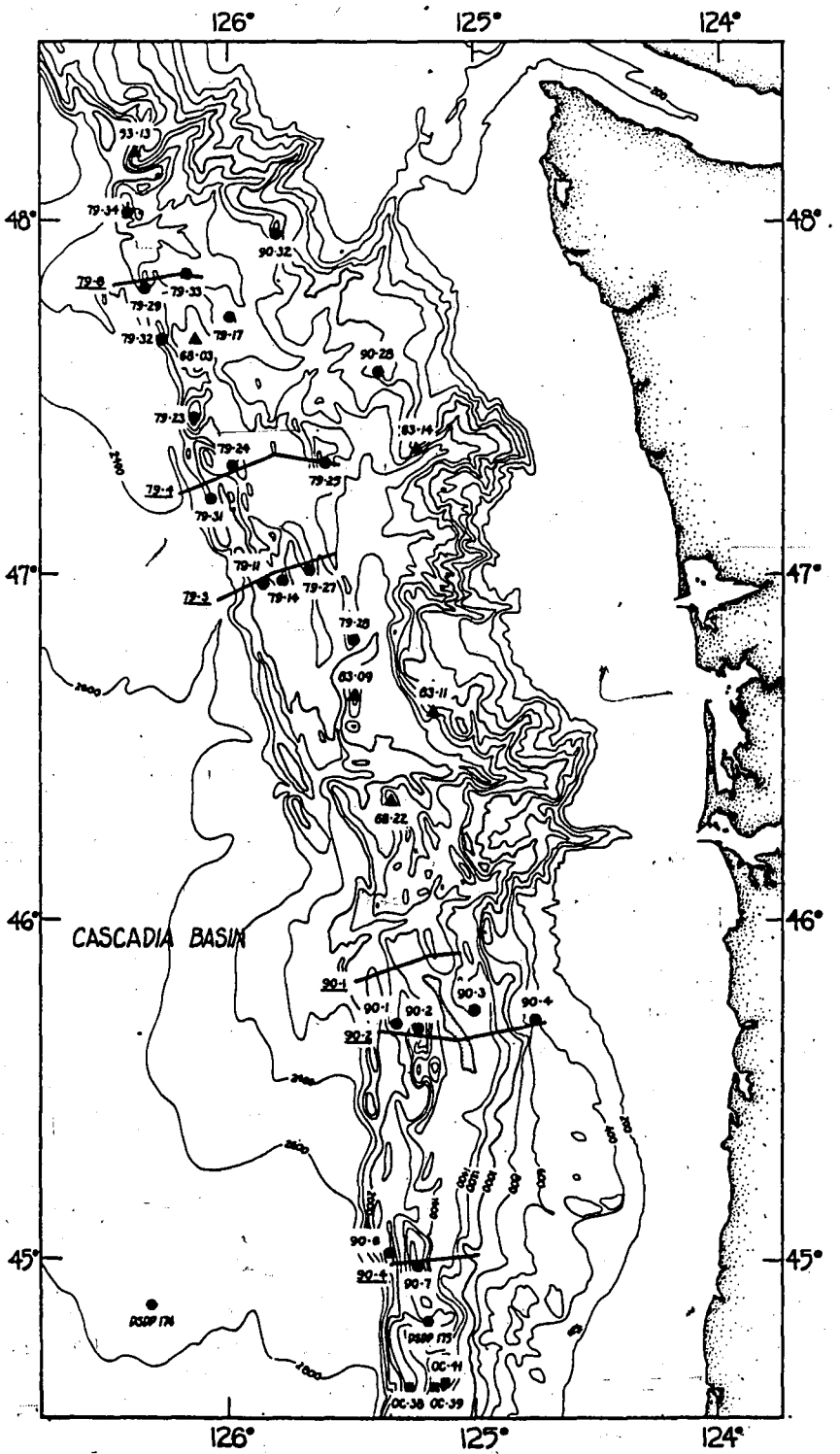

Figure 1: Bathymetric Map of Washington-Oregon Lower Slope Showing Dredge Sample Locations and Seismic Profiles (Carson, 1977).

1974; Carson, 1977).

The samples used in this study came from sites 79-31 and 79-28 (fig. 1). The former is located on the westernmost ridge while the latter lies 30 km to the east and south. The mud deformed in the laboratory was prepared from sample 79-14, located approximately midway between the other two samples.

Rates of subduction calculated by several methods are all in reasonable agreement: Atwater (1970), 2.6 cm/yr; Silver (1972), 2.0 cm/yr; von Huene and Kulm (1973), 1.6 to 2.7 cm/yr; Carson (1977), 2.3 to 2.9 cm/yr. Assuming a mean rate of 2.3 cm/yr, sample 79-28 must then be approximately 1.3 million years older than sample 79-31, which (sample 79-31) is of late Pleistocene age (0.3×10^6 years).

There are several indications that the samples used in this study have never been deeply buried. The collection procedure (dredging) insured that samples were taken only from the surface, and seismic profiles (Carson et al, 1974) indicated that slumping has been minimal. Thus it may safely be assumed that mineral orientations (other than parallelism with bedding planes) determined in this study are the result of mechanical, tectonic consolidation only. This conclusion if confirmed by the physical properties (Table I) of the sediments (Carson, 1977).

TABLE I: PHYSICAL PROPERTIES OF MUDSTONES

Specimen:	79-31	79-28
Water Content: (percent dry weight)	29.77	24.87
Max. Past Pressure: (T/M^2)	250	330
Shear Strength: (kg/cm^2)	4.25	3.90

METHODS

EXPERIMENTAL DEFORMATION.

A squeezebox apparatus was designed by Drs. Bobb Carson and Terrance J. Hirst to simulate initial horizontal compression and concomitant dewatering of deep sea sediments involved in subduction. The squeezebox consists of a plexiglass trough (inside dimensions: 125 cm long x 20.2 cm wide x 20 cm high) in which a plate at one end moves horizontally. The plate is driven by rack and pinion gears and a synchronous motor coupled through two gear reducers (1000:1 and 200:1). Interchangable motors allow the selection of various final drive rates, with those available for this experiment yielding rates of 99.7, 9.97, and 0.997 μcm/s. The intermediate rate was selected for this experiment, being only two orders of magnitude greater than the natural convergence rate

for this area and confining the experiment to a reasonable length of time. This rate results in a strain rate of 1.1×10^{-7} s^{-1}.

Bulk density (Myers et al, 1974) and thus water content (Richards et al, 1974) of the sediment in the squeezebox is measured by gamma ray attenuation. A steel frame surrounding the box holds the gamma ray unit which consists of a Cs^{137} source on one side of the box and a scintillation detector on the other. Gamma rays passing through the box are counted by a multichannel analyzer, and the system is calibrated by scanning solutions of known densities which bracket those found in the sediment. The gamma ray unit rides horizontally on two rails which are adjustable vertically at 1.9 cm increments; thus an array of regularly spaced points can be monitered repeatedly.

A slurry of mud (disaggregated mudstone from site 79-14; 59 percent silt, 41 percent clay, and less than 1 percent fine sand, and deaired Instant Ocean) with an initial water content of approximately 90 percent (dry weight) was installed in the box to a depth of ~ 12 cm and deaired with a concrete vibrator. The sediment was then submerged in Instant Ocean, and allowed to passively consolidate (to 10 cm) for two weeks. The mean water content following consolidation was 87 percent.

Following the consolidation period, the mud was deformed by horizontal compression over a period of 431.3 hours, with a total shortening of 15.4 cm (overall e= 0.171). During this time water contents were monitered and line drawings and photographs of the fracture patterns were made approximately every 24 hours.

SAMPLING PROCEDURE.

Dredged Samples. Inspection of twenty-six original dredge samples indicated that thirteen exhibited macroscopic evidence of foliation (hackly parting, fissility on subparallel planes; Carson, personal communication). These specimens were closely examined for presence of cleavage by binocular microscope and two samples were selected for further study. These samples were trimmed to remove disturbed portions, and two orthogonal cuts were made in each, one normal to and one parallel with a reference axis defined by the bedding-cleavage intersection. (This orientation was not strictly adhered to in the case of sample 79-31; this is due to the fact that the foliation in this sample was discovered on the faces of saw cuts made previously for another purpose. This set of cuts was orthogonal, and within 15° of the proper orientation; as the sample was relatively small and fragile, it was decided to use it as cut.) Thin

sections, x-ray transmission sections, and SEM mounts were subsequently prepared from the cut surfaces.

Artificially Deformed Samples. The squeezebox mud was cored, following deformation, at three locations: sample number 5-1, 3 cm from the plate (surface of active convergence); sample number 5-2, 16 cm from the plate; and sample number 5-4, 56 cm from the plate. Thin walled 4 cm (ID) plastic tubing was used for the cores with the cutting edge beveled to minimize disturbance. These cores were sealed in plastic bags until subsequent impregnation.

Following the completion of squeezebox deformation, and prior to removal of cores, vane shear strength determinations were made at 5 cm intervals along the length of the box. The tests were performed with a standard Wykham-Farrance vane shear apparatus in accordance with ASTM standards (rotation at approximately 20°/ min). The apparatus consisted of a 2.54 cm vane, driven through a strain transducer by a small motor mounted on a frame which allowed the vane to be slowly lowered into the mud. The transducer was connected to an x-y recorder, and the system was calibrated by hanging weights from a flywheel (5.6 cm in diameter) inserted into the vane chuck.

SAMPLE PREPARATION.

Petrofabric studies on unlithified sediments must deal with the inherent problem of fabric alteration by

sample extraction and preparation. This difficulty was exacerbated in this study by the high water contents of the squeezebox sediments; since the SEM operates in a vacuum, samples must be absolutely dry, and since both x-ray goniometry and thin sectioning require grinding and polishing, the fabric must usually be fixed by an impregnating medium. Unfortunately, sediment fabrics, especially those of clays, can be disrupted by removal of water (due to increases in surface tension) and impregnation.

An impregnation technique for wet sediments was developed by Mitchell (1956) which causes only minimal fabric disturbance. The impregnating medium is a high molecular weight polyethylene glycol (Carbowax 6000), which is water soluble, melts at 55° C., and has a hardness of one on Moh's scale. The sample is immersed in a bath of molten Carbowax (at 60° C), which replaces the pore fluid by diffusion. Once impregnation is complete, the sample is removed from the oven and allowed to harden, whereupon it may be cut and ground normally, with the exception that kerosene or some other organic solvent must be used as a lubricant. The time necessary for completion of impregnation is a function of porosity, permeability, and length of the diffusion path; squeezebox cores 5-1 and 5-2 were impregnated for approximately 3½ months, while 5-4 was

left in the molten wax for an additional 1½ months. During the latter period, an unfortunate change occured in the composition of the wax such that it would not harden properly. It then became necessary to freeze this core (5-4) in liquid nitrogen prior to and during subsequent grinding operations.

A number of clay fabric studies have successfully used Carbowax impregnation, apparently without significant fabric alteration (Martin, 1966; Quigley and Thompson, 1966; Gillot, 1970; Tchalenko, Burnett, and Hung, 1971; Chawla, 1973). Quigley and Thompson (1966) measured volumetric shrinkage of 22 percent after Carbowax impregnation of clay with an initial water content of 78 percent (dry weight). This compares with a volume loss of 40 percent in a similar air-dried sample; furthermore, shrinkage was nearly the same parallel and perpendicular to the specimen reference axis, and thus could not augment or diminish any preferred orientation present. Kazi (1975) similarly measured volume losses of 4 to 5 percent and 6 to 10 percent in Carbowax-impregnated clays with initial water contents of 35 and 51.4 percent respectively. Martin (1966) found no significant difference in x-ray fabric determinations on identical samples, one impregnated with Carbowax, and one frozen in liquid nitrogen. Gillot (1970) found that x-ray

fabric determinations differed somewhat among samples that were freeze-dried, critical point-dried, and impregnated in Carbowax®, but these differences were small compared to the effects of air drying. In the present study, linear structures such as shear planes were observed to be apparently undisturbed by Carbowax impregnation. In particular, one sample contained a major shear fracture along which the core separated upon extraction. The surfaces of this fracture remained planar following the Carbowax impregnation.

Following impregnation, the squeezebox cores were cut on two orthogonal planes, both parallel with the axis of compression (the long dimension of the box), one horizontal, and one vertical. From these surfaces, thin sections and x-ray transmission sections were prepared. While thin sections were prepared in the normal manner, the x-ray transmission sections were prepared by scraping and shaving slices to the proper thickness with the edge of a glass slide. (This technique was suggested by Dr. David Baker; personal communication).

While the water contents of the mudstone samples were too low to allow effective impregnation by Carbowax, they were also low enough to allow air-drying without significant damage to fabric; these samples, when dried, contained none of the closely space dessication cracks

typical of air-dried samples of higher initial water contents. Once dry, they were impregnated under vacuum with Scotchcast Resin #3 (Minnesota Mining and Manufacturing Co., Philadelphia, Pa.), a low viscosity (100 cps @ 95° C) epoxy resin developed for impregnation of finely-wound electronic coils.

X-RAY POLE FIGURE GONIOMETRY.

The technique of x-ray pole figure goniometry was originally developed for the study of textures in metals (see Barrett and Massalski, 1966). It was first used in geological investigation by Means and Patterson (1966) and attained its current level of refinement with the work of Baker, Wenk, and Christie (1969). It has since been utilized in numerous studies of preferred orientations in slates (Oertel, 1970; Tullis, 1971; Oertel and Curtis, 1972; Tullis and Wood, 1975; Siddans, 1976; Wood et al, 1976); schists (Lipshie, Oertel, and Christie, 1976); and experimentally deformed clays (Martin, 1966; Chawla, 1973) and mica aggregates (Means and Patterson, 1966; Tullis, 1971).

In the current study, a modified Seimens pole figure goniometer at Brown University's Department of Geological Sciences was used to obtain pole figures of the chlorite 001 plane ($d = 7\text{Å}$, $2\theta = 12.5$, Cu $K\alpha$) for three

squeezebox cores and one mudstone. The instrument modifications are described in Holeywell and Tullis (1975), and were made to allow motorized 2θ scans and automated spiral scanning of the pole figure.

The process of x-ray pole figure goniometry involves initial 2θ scans for selection of a suitable peak (one which is well defined and free of interference from neighboring peaks). The aperture and detector are then set to the desired 2θ angle, and the specimen is scanned while rotating about its normal axis (β revolution, fig. 2). During this rotation, the specimen normal is slowly tilted (τ tilt, fig. 2) in the plane of the x-ray beams at the rate of 2.5 degrees per full β revolution. As the specimen rotates in this manner, the continuously recorded diffraction intensity is a function of the 001 pole density for a given specimen orientation. The trace of the scan defines a spiral on the pole figure (lower hemisphere equal area projection, fig. 3).

Two modes of operation are possible with the pole figure device: reflection and transmission. In the reflection mode, the specimen normal bisects the angle formed by the primary and diffracted beams. In the transmission mode, the plane of the specimen bisects this angle. Since the instrument allows a maximum τ tilt of 40°, coverage of the complete pole figure requires a combination

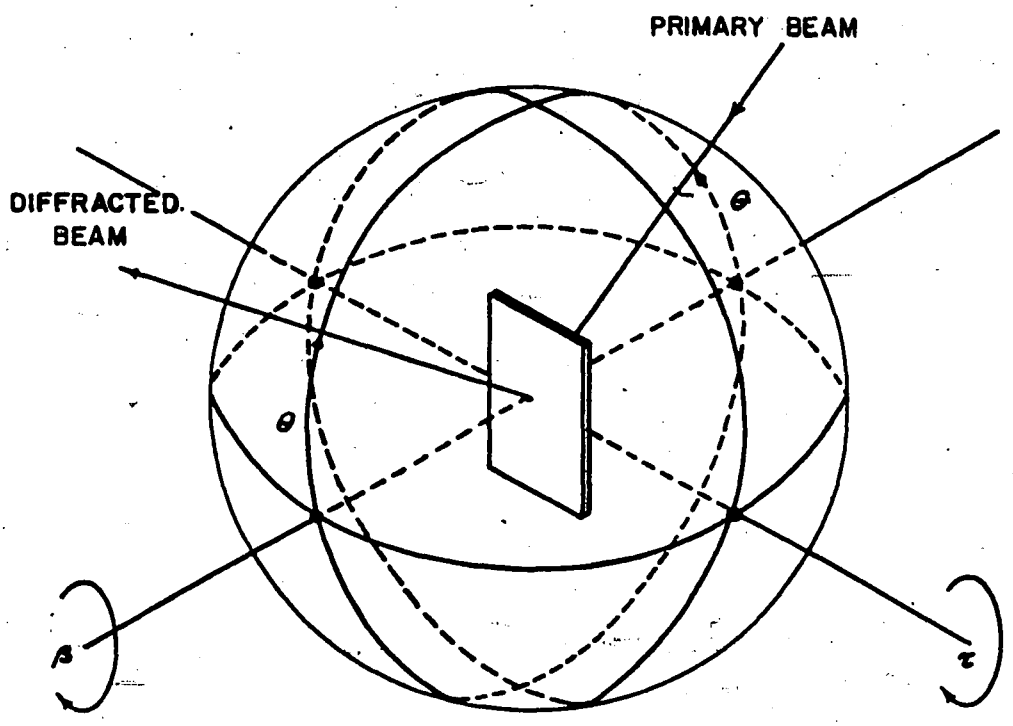

Figure 2: Pole Figure Goniometer Geometry.

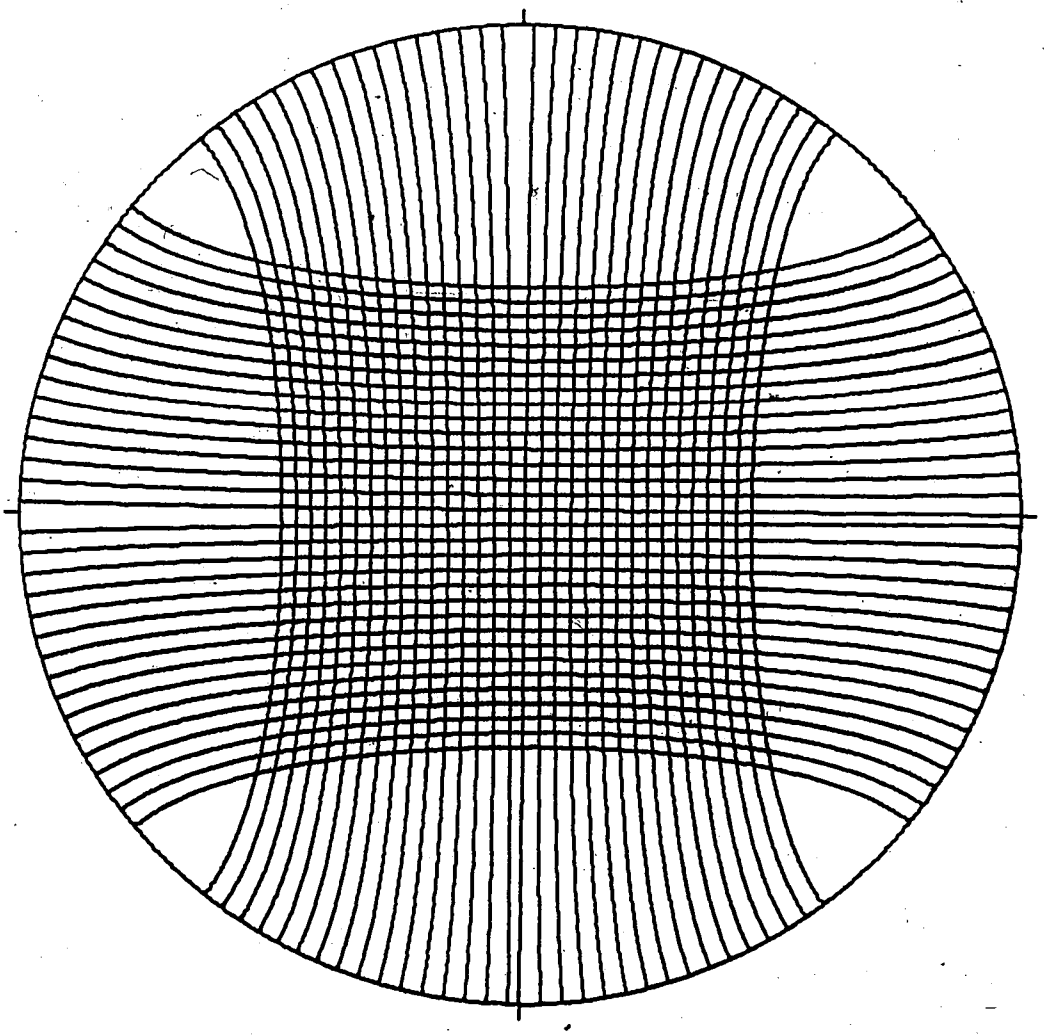

Figure 3: Computer Generated Diamgram of Coverage of Pole Figure with Two Perpendicular Spiral Scans.

either one reflection and one transmission scan, or transmission scans of three orthogonal sections. Since serious defocusing of the beam occurs in reflection at low 2θ values (Baker, Wenk, and Christie, 1969), transmission was used exclusively in this study. Although three transmission scans are required for complete coverage, the use of two scans, if both are made on sections cut perpendicular to cleavage (Wood et al, 1976) will leave four 10^{o} x 24^{o} triangular areas on the periphery of the pole figure (fig. 3). When it can be ascertained that no critical information will be lost in these areas, two scans are sufficient (Oertel and Curtis, 1972).

The proper thickness of a transmission specimen is one that will cause attenuation of the x-ray beam by $e^{-\mu t}$, where $\mu t = 1$; μ is the linear absorption coefficient, and t is thickness. This thickness for most rock materials is 100 μm; in this case, owing to the high porosity and fragility of the specimens, specimen thickness was held to a range of 155 to 236 μm. These specimens still gave acceptable values of μt (see Table II).

Spiral scans were run on two perpendicular sections each from mudstone 79-31 and three squeezebox cores. Beta revolution was at a rate of 12 degrees/min., each scan lasting 8 hours. Instrument and panel settings are given in Table III.

TABLE II: μt VS. THICKNESS

Specimen	Thickness(μm)	μt
79-31	188	1.339
5-1-2	205	1.116
5-1-3	208	1.002
5-2-2	188	0.914
5-2-3	236	1.304
5-4-2	155	0.905
5-4-3	173	0.943

TABLE III: X-RAY INSTRUMENT SETTINGS

	Kv	40
	Ma	30
Slits:	Aperture	1.0 x 2.4 mm*
	Detector	2.5 x 7.0 mm
	Filter	Ni
Detector Voltage		1000
Rate Meter:	Range	5000
	Time Constant	10
Pulse Height Analyzer:	Base	0.6
	Window	3.0

* + 2 mm collimator

The intensity recorded on the stripchart is the sum of background and net intensity. Background was measured by running 2θ scans at a β value which gave low total intensity, one at $\tau = 0^{\circ}$ and one at $\tau = 40^{\circ}$. Background could then be interpolated under the diffraction peak.

As the specimen tilts (increasing τ), a greater volume is irradiated and thus absorption increases. Tullis (1971) thus found it necessary to use a background correction:

$$Bg_{\tau}/Bgo = \exp(\mu t(1/\cos\theta - 1/\cos(\tau-\theta))) \qquad (1)$$

where: Bg_{τ} = background at tilt τ

Bgo = background at zero tilt

τ = tilt angle

θ = Bragg angle.

Baker, Wenk, and Christie (1969) and Chawla (1973), however, used no tilt correction. In this study, both background total intensity were found to decrease with tilt, and the best agreement between plotted pole figures and strip charts was obtained through use of a correction (Decker, Asp, and Harker, 1948) for total raw intensity:

$$Icorr = Iobs((\mu t \exp(-\mu t/\cos\theta)/\cos\theta)(\cos(\theta-\tau)/\cos(\theta+\tau)-1)/(\exp(-\mu t/\cos(\theta-\tau))-\exp(-\mu t/\cos(\theta+\tau)))) \qquad (2)$$

where: Icorr = corrected intensity

Iobs = observed intensity

μt, θ, τ as defined above in (1)

The value of μt used in this formula was determined by substitution of observed background ratios (Bg_{40}/Bg_0) into equation (1)

The strip charts from the spiral scans were digitized with a Talos cybergraph. The digital points were fed into a Tektronix 4051 desk-top computer, and interpolated at 24 second ($4.8^{\circ}\beta$) increments. The interpolated data were processed by a program (Berglund, 1978) which transforms instrument coordinates into specimen coordinates, subtracts background, corrects intensities for absorption changes due to tilt (equation (2), above), and plots net intensities in equal area stereographic projection.

The resultant pole figure must then be normalized in multiples of a random distribution of poles. The technique outlined by Tullis (1971, p 69) was followed: A rough estimate of random intensity (that intensity expected in a sample with random fabric) is made, and a provisional pole figure prepared, contoured in multiples of the estimated random intensity. The pole figure is then integrated by measuring areas between contours with a polar planimeter and multiplying each area fraction by its mean intensity. For a properly normalized pole figure, the integral (Σ(area fraction)(mean intensity)) should equal one; the

correct random intensity is thus found by multiplying the estimate by the value of the integral. The correctly normalized pole figure can then be plotted.

SCANNING ELECTRON MICROSCOPY.

The scanning electron microscope (SEM) was used extensively in this study to ascertain the microstructure of the foliation in specimen 79-31. Attempts to examine freeze-dried squeezebox mud samples, however, proved unsuccessful. The extremely high porosities of these specimens prevented complete coating of the specimen surface, resulting in charging by the electron beam and consequently extremely poor image quality. Mudstone specimens were prepared by fracturing air-dried specimens, blowing clean the fractured surface, and coating with a thin (several hundred Å) layer of carbon in a vacuum evaporator.

THIN SECTIONS.

While clay-sized paricles are usually not resolvable with the optical microscope, the phenomenon of aggregate extinction makes thin sections quite useful in the study of argillaceous fabrics. Furthermore, since all clays and micas are optically length-slow (parallel to the basal plane), examination under crossed nichols with the gypsum

plate (λ) reveals preferred orientation by color (green if perpendicular to the slow ray of the gypsum plate and yellow if parallel); qualitative intensity of the preferred orientation is indicated by the purity or uniformity of the color. Observation of thin sections also allows viewing of much larger areas than those seen with the SEM, and the planar nature of thin sections makes them most useful for the determination of larger scale structures.

Thin sections were prepared in the normal manner, with two exceptions: First, as Carbowax is water soluble, sections from the squeezebox had to be ground in kerosene. Second, since Carbowax melts at 55° C. and Scotchcast epoxy softens at 100° C., Lakeside could not be used for bonding in either case. Hillquist thin section epoxy was selected as an alternative; it cures at room temperature in 24 hours. This epoxy, however, proved an unfortunate choice; one part of the mixture was found (after preparation of the thin sections) to be contaminated with minute (~20μm) rhombic crystals, which become increasingly visible and annoying in areas where the section tapers to minimum thickness, precisely the regions where resolution of small grains is optimal. An additional problem associated with this epoxy is its tendency to form bubbles upon mixing which are not readily released thereafter.

RESULTS

EXPERIMENTAL DEFORMATION.

The stuctural configuration of the sediment mass is shown before, during, and after experimental deformation in figure 4. Within 24 hours of the onset of squeezing (z = 0.8 cm; z is horizontal travel of squeezing plate), shearing developed within 12 cm of the plate on planes dipping variously 10° to 30° toward the plate. These fractures continued with time to propagate away from the plate; by 73.1 hours (z = 2.6 cm), a series of short (2-20mm) en echelon shear fractures had developed with the same attitude. The first shearing on planes dipping (at 20°) away from the plate developed by 95.8 hours (z = 3.35 cm); these fractures lengthened until at 143.4 hours (z = 5.05 cm), there was roughly an equal distribution of fractures dipping in each direction. Over the next several days of the experiment, however, movement on planes dipping toward the plate began to dominate; by 214.0 hours (z = 7.6 cm), two major overthrusts, actually continuous sets of smaller fractures running from near the bottom of the box to the sediment surface, had developed. These planes, dipping 20° (the set closer to the plate) and 25° (the set further from the plate), were to accommodate much of the shortening during the balance of the experiment.

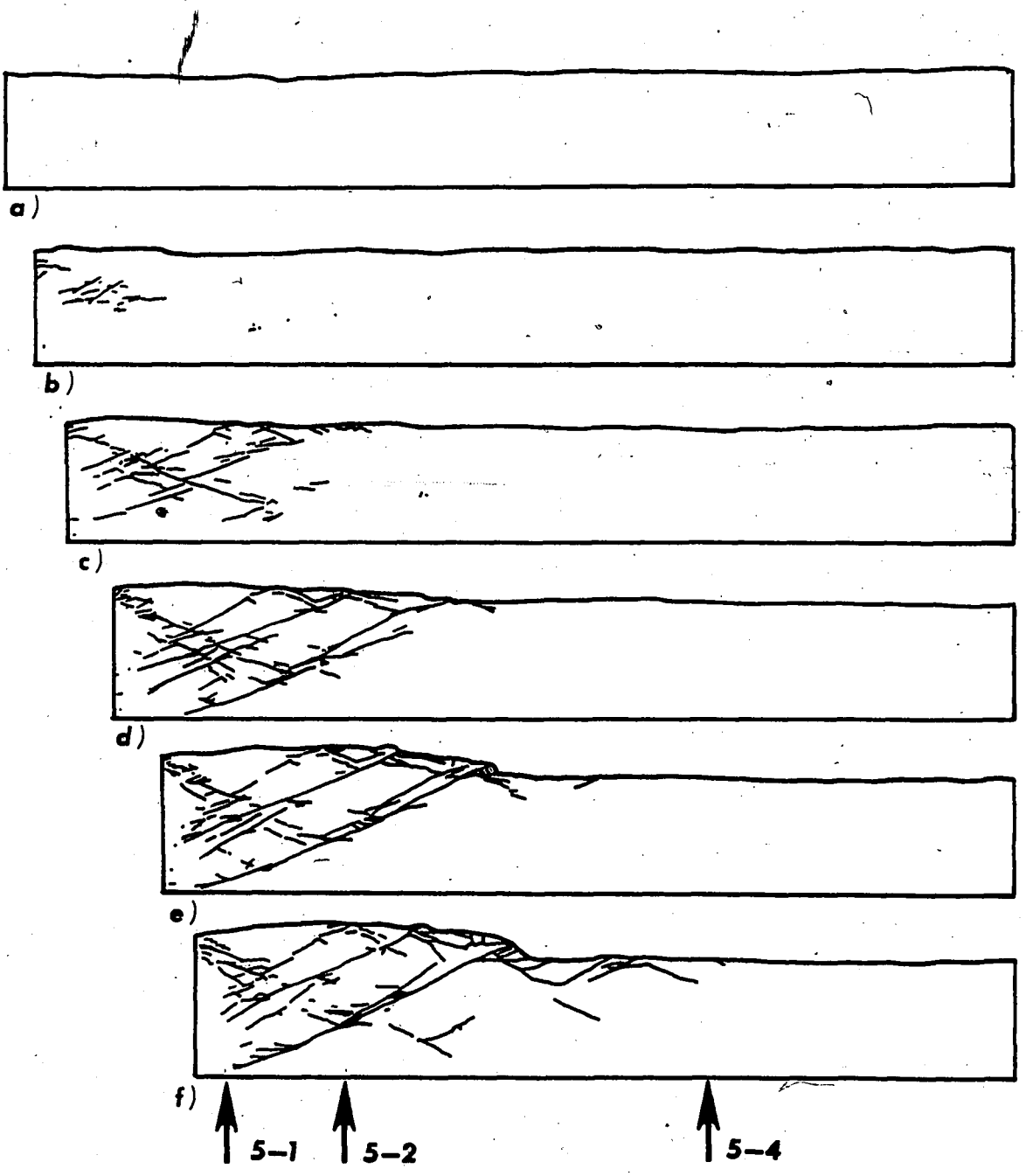

Figure 4: Squeezebox Deformation. a) Time (t) = 0, Distance Travelled by Plate (z) = 0; b) t = 73.1 hrs., z = 2.6 cm; c) t = 143.4 hrs., z = 5.05 cm; d) t = 246.7 hrs., z = 8.75 cm; e) t = 361.0 hrs., z = 12.85 cm; f) t = 431.3 hrs., z = 15.4 cm.

Additional shear displacements continued to appear, however, and some of the older fractures closed and all but disappeared as movement ceased at one point to be taken up at another. At 335.5 hours (z = 11.95), faulting had occured beyond the tip of the furthermost overthrust, along several planes dipping 25° away from the plate. These displacements developed further as movement continued along the overthrust. By the end of the experiment, faulting had extended 45 cm from the plate; final fault attitudes were 20° to 30°, dipping both toward and away from the plate in the vicinity of core 5-1; and 22° to 25°, dipping toward the plate, in the vicinity of core 5-2.

Total movement of the plate was 15.4 cm; this yields a total compressive strain value of -0.17.

Water loss ranged from a maximum of 30.6 percent (of original water content) 11 cm from the plate and 8 cm above the bottom of the box, to a minimum of 2.5 percent at the far end of the box, near the surface.

VANE SHEAR STRENGTH.

Vane shear strengths after deformation ranged from 1.54 kPa, closest to the plate, to 0.77 kPa at the far end of the box, showing a general decrease with increasing distance from the plate and increasing water content (fig. 5). The maximum vane shear strength measured is extremely

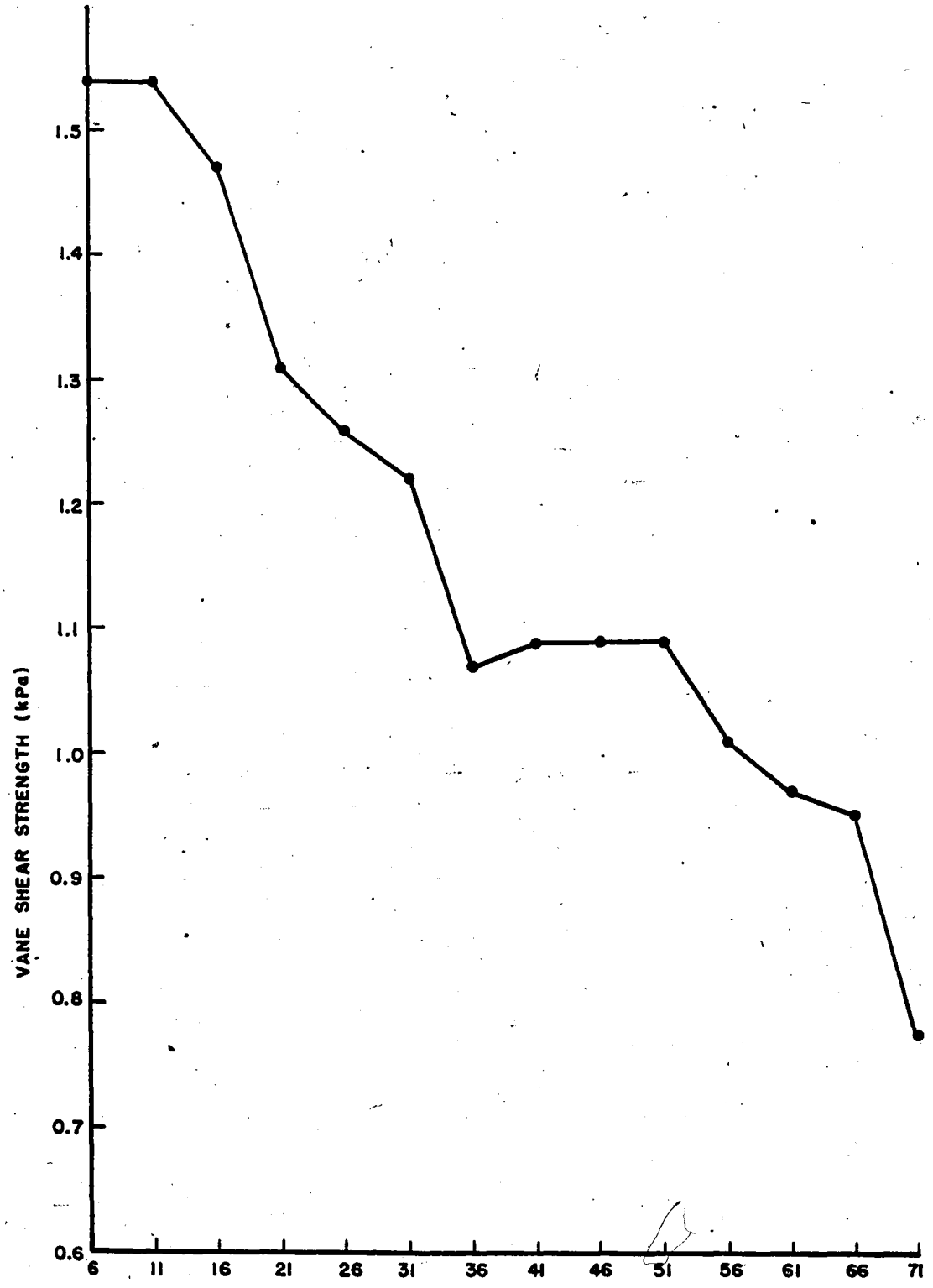

Figure 5: Vane Shear Strength vs Distance From Plate

low, however, indicating little resistance to shear strain.

SEDIMENT MICROSTRUCTURES INDUCED BY EXPERIMENTAL DEFORMATION.

The microstructure of the squeezebox sediment, as seen in thin section, is characterized chiefly by severe inhomogeniety; while some shear fractures may persist laterally for several centimeters, areas in which the fabric is homogeneous are rarely greater than 20 mm^2 in areal extent.

Two types of structures are common: shear fractures (plates 1, 2, 3, 4), and a domainal structure consisting of narrow, lenticular, alternating domains in which clays are inclined in opposite directions to the axis of the domain (plates 5, 6, 7, 8, 9, 10, 11, 12). These latter structures are referred to in the literature as crenulations (Maltman, 1977) when the alternate bands are symmetrical, and kink bands when one set of domains dominates and the inclination angles differ markedly (Maltman, 1977; Morganstern and Tchalenko, 1967; Tchalenko 1968). This terminology will be used here; crenulation, however, is not to be confused with crenulation cleavage, for although these crenulations are somewhat similar morphologically to that type of cleavage, they lack the axial

planar cleavage characteristic of true crenulation cleavage.

The crenulations consist of lenticular domains, rarely longer than 5 mm, which, when viewed with crossed nichols and gypsum plate, appear as yellow and green stripes (light and dark zones in plates 5, 6, 7, 8, 9, 10, 11, 12) owing to opposite orientations within alternate domains. They are most commonly oriented parallel to the trace of the xy plane (plane parallel to plate - x is vertical, positive downward; y is horizontal, positive toward the front side of the box; and z is horizontal, the direction of compression). Less often, they are inclined at small angles ($\leq 15^{o}$) to the x and y axes, and occasionally can be found nearly parallel to the z axis (plate 4). Angles between aligned clay flakes and domain axes in the latter case, however, are usually less symmetrical.

The internal angle formed by the junction of clay flakes in the crenulations varies from 60^{o} to 100^{o}; the width of the individual domains is equally variable, ranging from 20 μm (plates 1 and 7) to as much as 300 μm (plate 10).

Shear fractures (macro- and microfaults) are pervasive in the squeezebox mud and are largely responsible for the inhomogeneity of the fabric. They are commonly

inclined 25° to 35° to the z axis, but in some cases this angle is as high as 45° or as low as 0°. They occur in four size classes, characterized by length, width of shear zone, and spacing between adjacent faults:

(1) Macrofaults, those observed with the unaided eye and traced during the progress of deformation. These faults are up to 1 mm wide, range from less than one to greater than 10 cm in length, and are spaced on the order of 1 cm apart. "Gouge zones" are observed microscopically along some of these faults (plate 13). Faults of this class tend to make smaller angles with the z axis than do those of the other three classes, usually 20° to 25°.

(2) The second class of shear fractures, and those most commonly observed microscopically, range in width from 200 to 300 μm, are on the order of 1 cm in length, and are commonly spaced 300 to 500 μm apart. These fractures are frequently parallel, sometimes en echelon. Examples can be seen in plates 2, 3, 4, and 14.

(3) Faults of the third class are typically 50 to 60 μm in width, approximately 2 mm in length, and are spaced approximately 500 μm apart (plate 1).

(4) The smallest faults observed are 15 to 20 μm in width, some 200 to 500 μm in length, and are spaced 20 to 70 μm apart (plates 1, 15, 16). Sets of these faults are generally limited to areas of less than 1 mm^2; they are

observed even in core 5-4, taken 56 cm from the plate.

Within the outer portions of the gouge zones of the largest faults, clay flakes are oriented parallel to the direction of shearing (plate 28). In the central regions, however, they lie at a small angle (10° to 20°) to the plane of shearing.

This relationship is also observed in the second class of faults; within the shear zones, clay flakes are well oriented with a rake of 15° to 30° to the shear plane, while they are parallel to shearing along the borders of the zone (plates 2, 3, 14, 17). In the smallest two classes of faulting, however, due to the extremely narrow width of the shear zones, all of the clays are seen to lie parallel to the shear surface (plates 1, 15, 16).

Some shear zones are observed which do not form well-defined displacement discontinuities; these are manifested as small areas in which the preferred orientation is the direction of shearing. This type of structure may sometimes be seen as limbs of asymmetric crenulations, and as incipient faults nearly parallel to the z axis (plate 4).

In addition to crenulations and shear fractures, a third type of structure is occasionally seen. Within each of the thin sections from cores 5-1 and 5-2,

areas are observed with the "expected" preferred orientation, i.e., normal to the z axis of the squeezebox. These areas commonly contain narrow crenulations. Examples are shown in plates 18 and 19.

POLE FIGURES: EXPERIMENTAL DEFORMATION.

Due to the severe inhomogeneity of strain within the squeezebox mud, it was impossible to combine partial pole figures from orthogonal sections of the same core. Furthermore, the measured preferred orientations did not coincide with those expected, and consequently, in most cases, maxima lie at the periphery of the region covered by scanning a single section. As a result of these two conditions, much information was lost, and it is not possible to determine absolutely the maximum pole density in each case. The partial pole figures, however, remain quite useful for determination of both the direction and character of the preferred orientations observed.

The partial pole figures are presented in figures 6 through 11. The maxima on the pole figures indicate preferred orientation poles as seen from the plate of the squeezebox, looking toward the fixed end (positive z axis direction). Contours are in multiples of a random distribution of poles, and the maximum intensity of the preferred orientation is given as "maximum pole density".

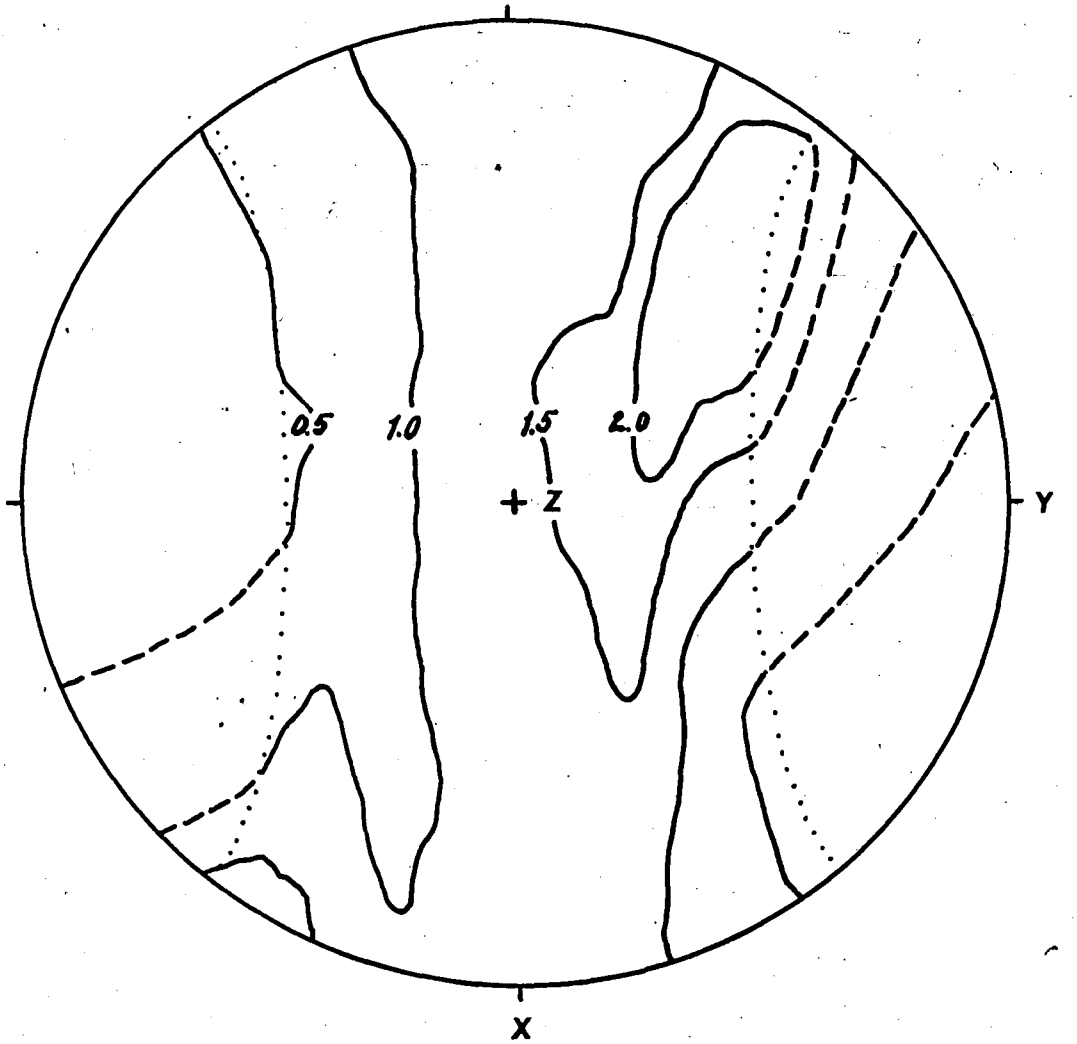

Figure 6: Partial Pole Figure for Sample 5-1-2. Maximum Pole Density = 2.8. Dotted lines indicate limits of spiral scan. Numerical suffix for sample indicates plane scanned: 2 is the xz plane (vertical), and 3 is the yz plane (horizontal); both planes are perpendicular to the plane of the plate. X is vertical, positive downward, Y is horizontal, positive toward the front of the box, and Z is the direction of compression.

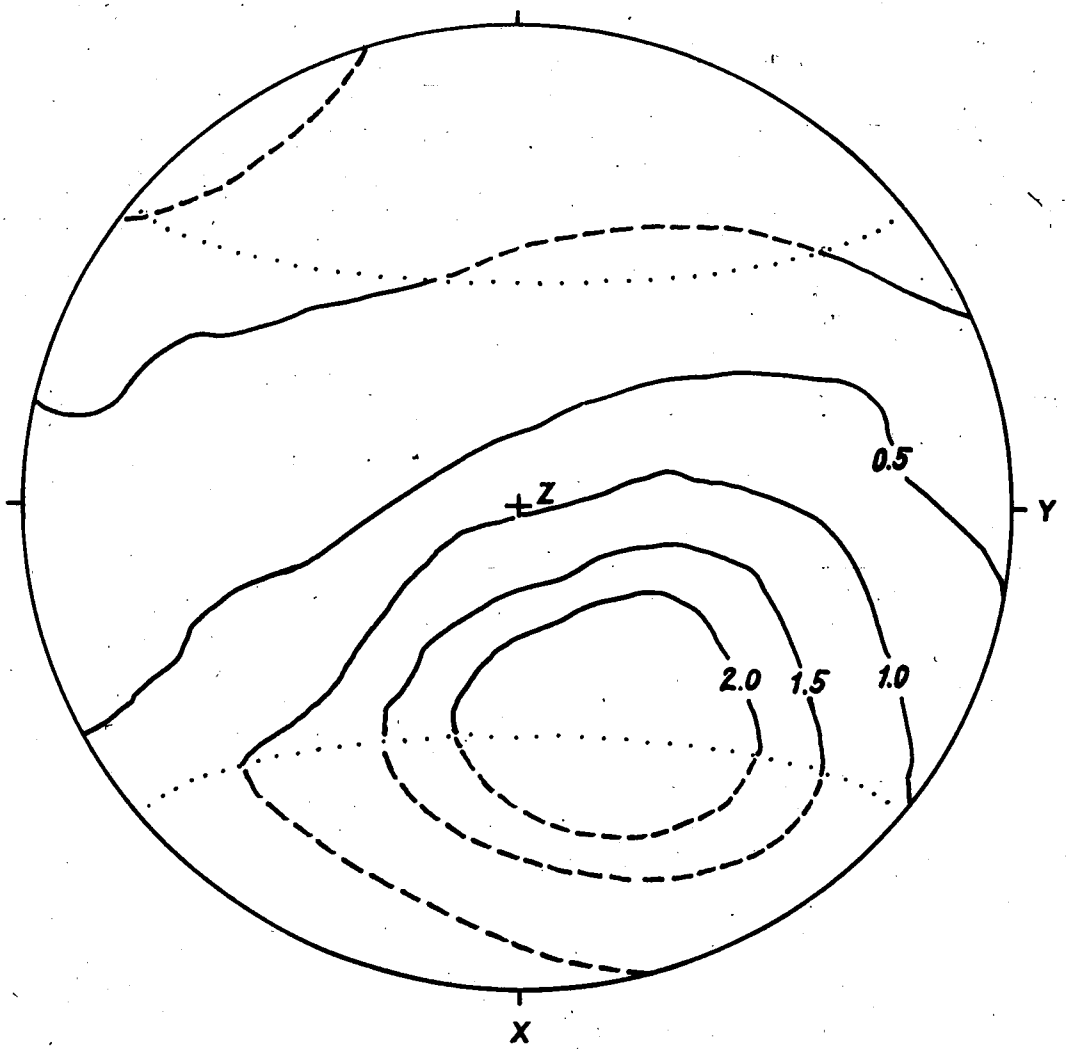

Figure 7: Partial Pole Figure for Sample 5-1-3.
Maximum Pole Density = 2.9.

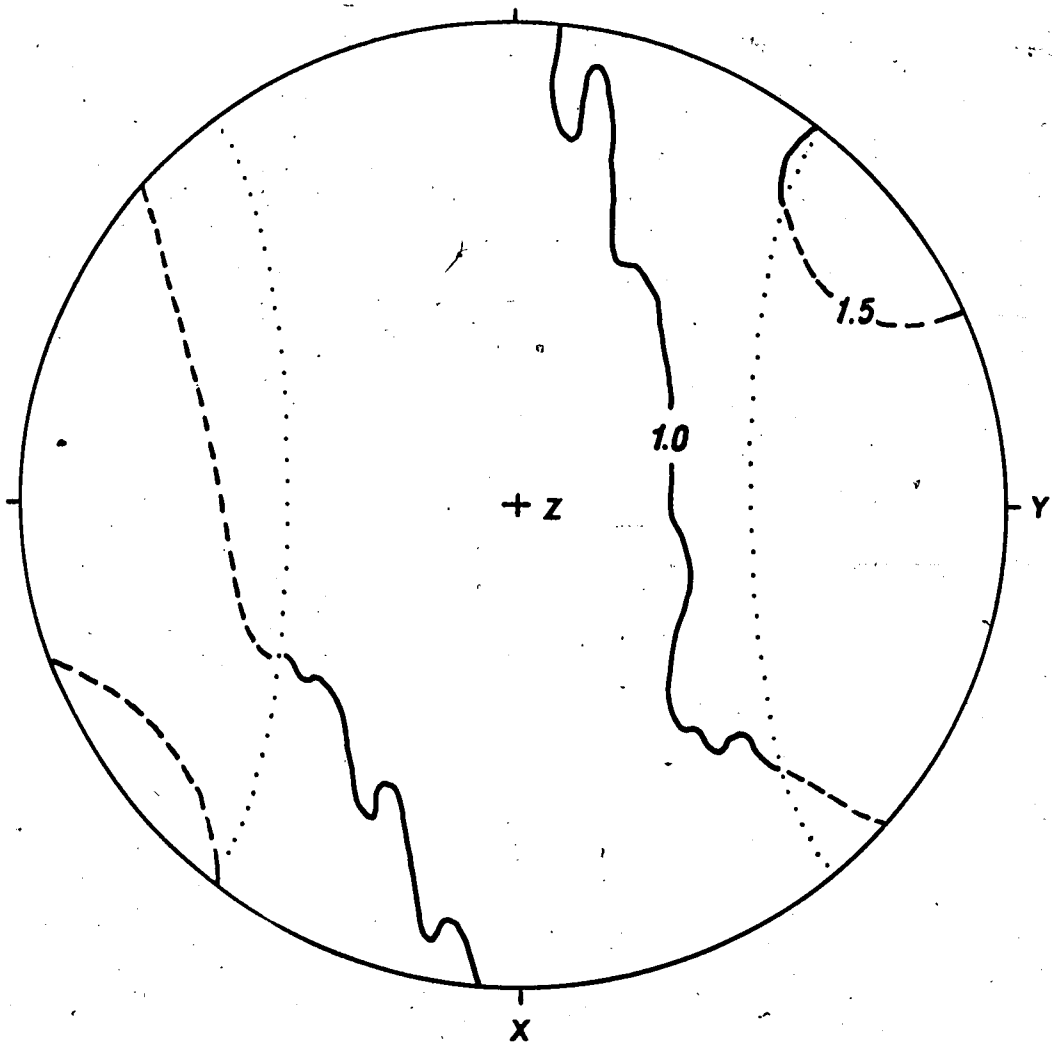

Figure 8: Partial Pole Figure for Sample 5-2-2.
Maximum Pole Density = 1.5.

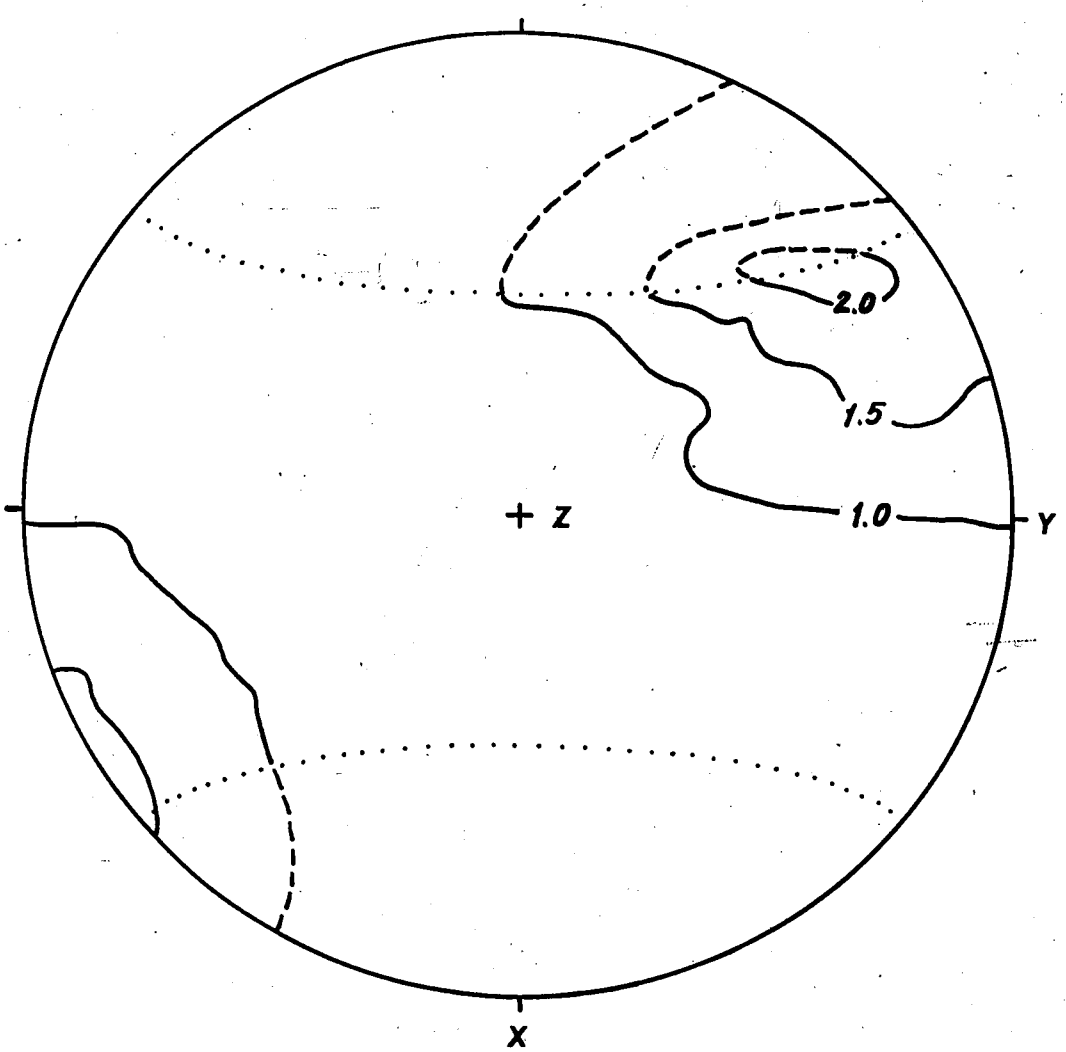

Figure 9: Partial Pole Figure for Sample 5-2-3. Maximum Pole Density = 2.1.

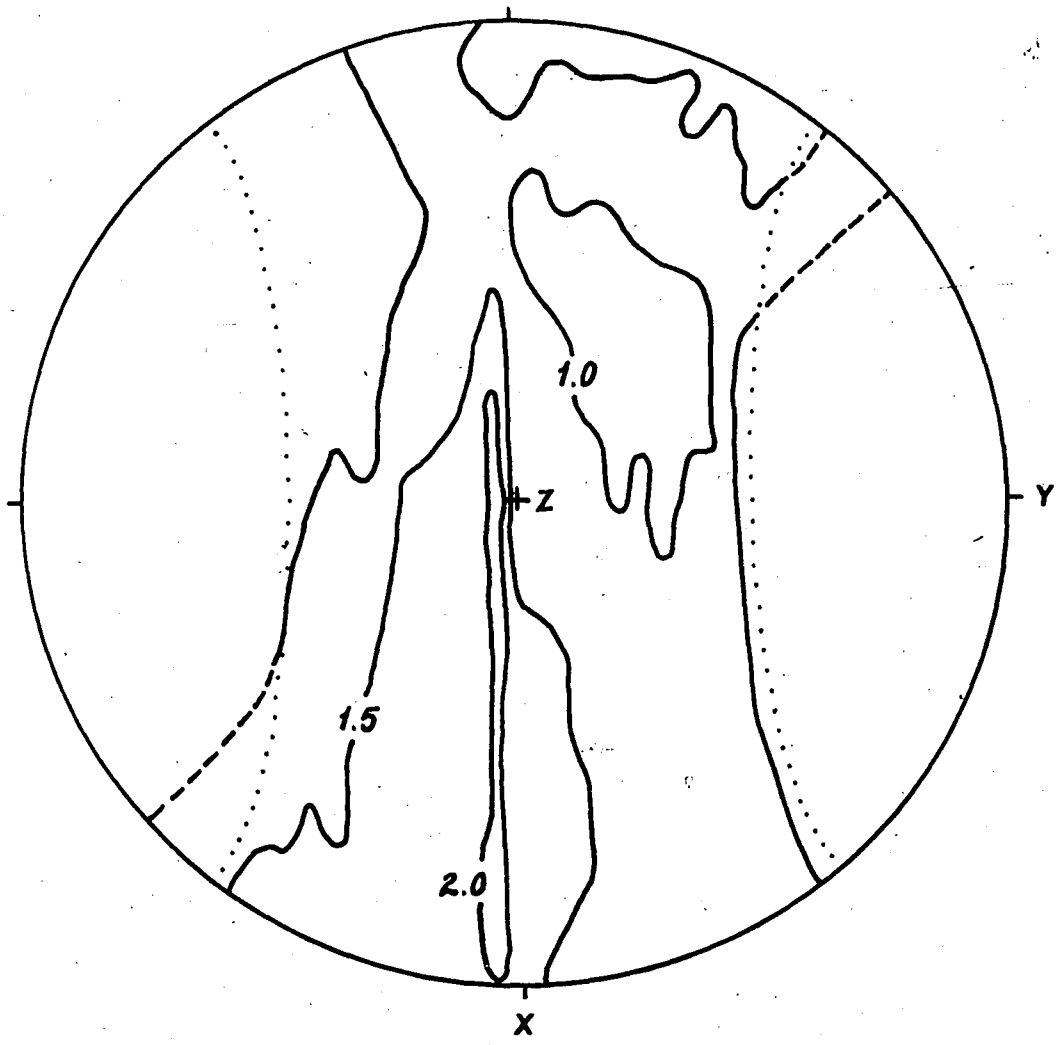

Figure 10: Partial Pole Figure for Sample 5-4-2.
Maximum Pole Density = 2.3.

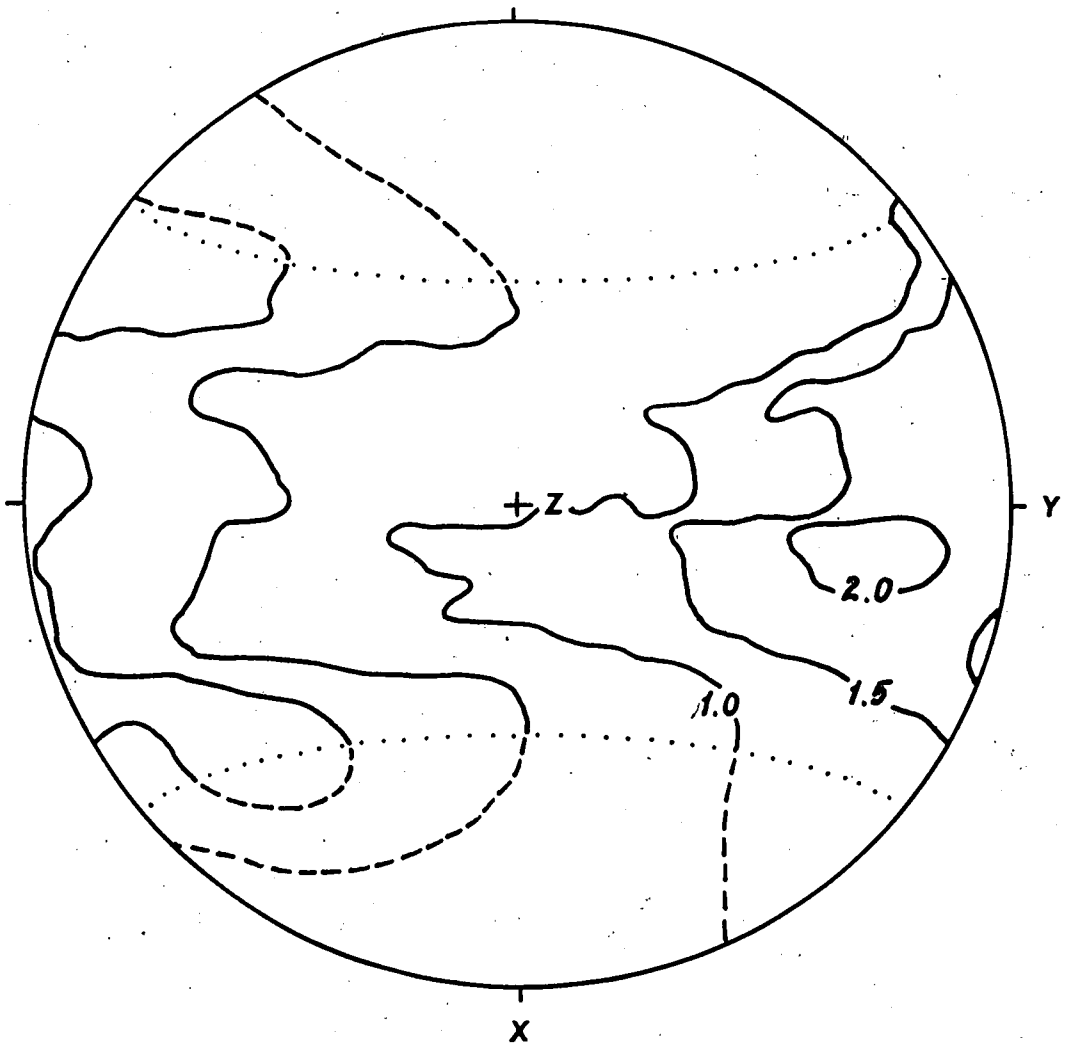

Figure 11: Partial Pole Figure for Sample 5-4-3.
Maximum Pole Density = 2.3.

The highest degree of preferred orientation was found in the sample closest to the plate (core 5-1). The vertical (fig. 6) and horizontal (fig. 7) sections of this sample exhibit maximum pole densities of 2.8 and 2.9 respectively. For comparison, the bedding plane pole density for natural mudstone sample 79-31 is 2.8; a typical maximum pole density for slate is 16 to 18 (Tullis, 1971).

While the two sections of sample 5-1 show nearly equal magnitudes of preferred orientation, the positions of the poles differ by approximately 90°. This is presumably due to the previously mentioned inhomogeneity.

Sample 5-2 shows a significantly lower degree of preferred orientation, with maximum pole densities of 1.5 for the vertical section (fig. 8) and 2.1 for the horizontal section (fig. 9). The pole positions for the two sections of sample 5-2 are nearly coincident with that of sample 5-1-2 (vertical section, fig. 6). The shapes of the maxima, however, are dissimilar; while that for sample 5-1-2 (fig. 6) is elongate parallel to the xz (vertical) plane, that for 5-2-3 (fig. 9) is elongate parallel to the yz (horizontal) plane. Note that the contours containing the maxima for sample 5-2-2 (fig. 8) are almost completely dashed. The true maximum in this case lies outside the region covered by the x-ray scan and may

have a value somewhat higher than 1.5.

The pole figures for sample 5-4 (figs. 10 and 11) exhibit several features which cast some doubt upon the data obtained from this sample. First, the maximum pole density for each section is 2.3, higher than the maxima exhibited by sample 5-2, which was much closer to the plate. Second, the contours show far less concentricity than do those of all the other pole figures. Finally, the shape of the maximum for 5-4-2 (fig. 10), very long and very narrow, differs significantly from those of the other pole figures.

MUDSTONE MICROSTRUCTURES.

Sample 79-28 exhibits almost slate-like parting along bedding planes. Spacing of these parting planes varies from 1 to 6 mm, and they appear in thin section to be defined in part by changes in mean sediment grain size.

No pole figure was made of this sample; the degree of preferred orientation can be readily seen both macroscopically and microscopically. Binocular microscope observation reveals the larger micas to lie parallel to bedding fissility; in thin section (plate 20) mass extinction and illumination are well defined. At higher magnification, with the SEM, the preferred orientation

appears less perfect, being disrupted by silt particles, but the overall parallelism is still obvious (plate 21).

During initial examination of all of the dredge samples, inspection of a cut face of sample 79-31 revealed the presence of rudimentary spaced cleavage which in appearance is not unlike the "anastamosing pelitic folia" often referred to by Powell (1969) and others. Thorough investigation of this foliation thus became the central thrust in the study of the natural mudstones.

The foliation is defined by discrete planes inclined at an average of 80^{o} to bedding; these planes appear in hand specimen as faint (barely visible to unaided eye) lines which are somewhat darker than the surrounding sediment. Spacing between folia varies from 0.5 to 10 mm, and is typically 1.5 to 2.0 mm. The folia anastamose in three dimensions, locally thinning or thickening as branches join or part (fig. 12). The thickest folia can be followed for at least 10 cm, apparently limited only by the size of the sample.

Optical and scanning electron microscopy reveal these folia to be zones of subparallel phyllosilicate flakes. In width, they range from 150 μm to a minimum of 10 μm; the thinner zones are rather difficult to find on the 1 cm^2 surface of a typical SEM mount. The degree of parallelism within the zones is sometimes well defined

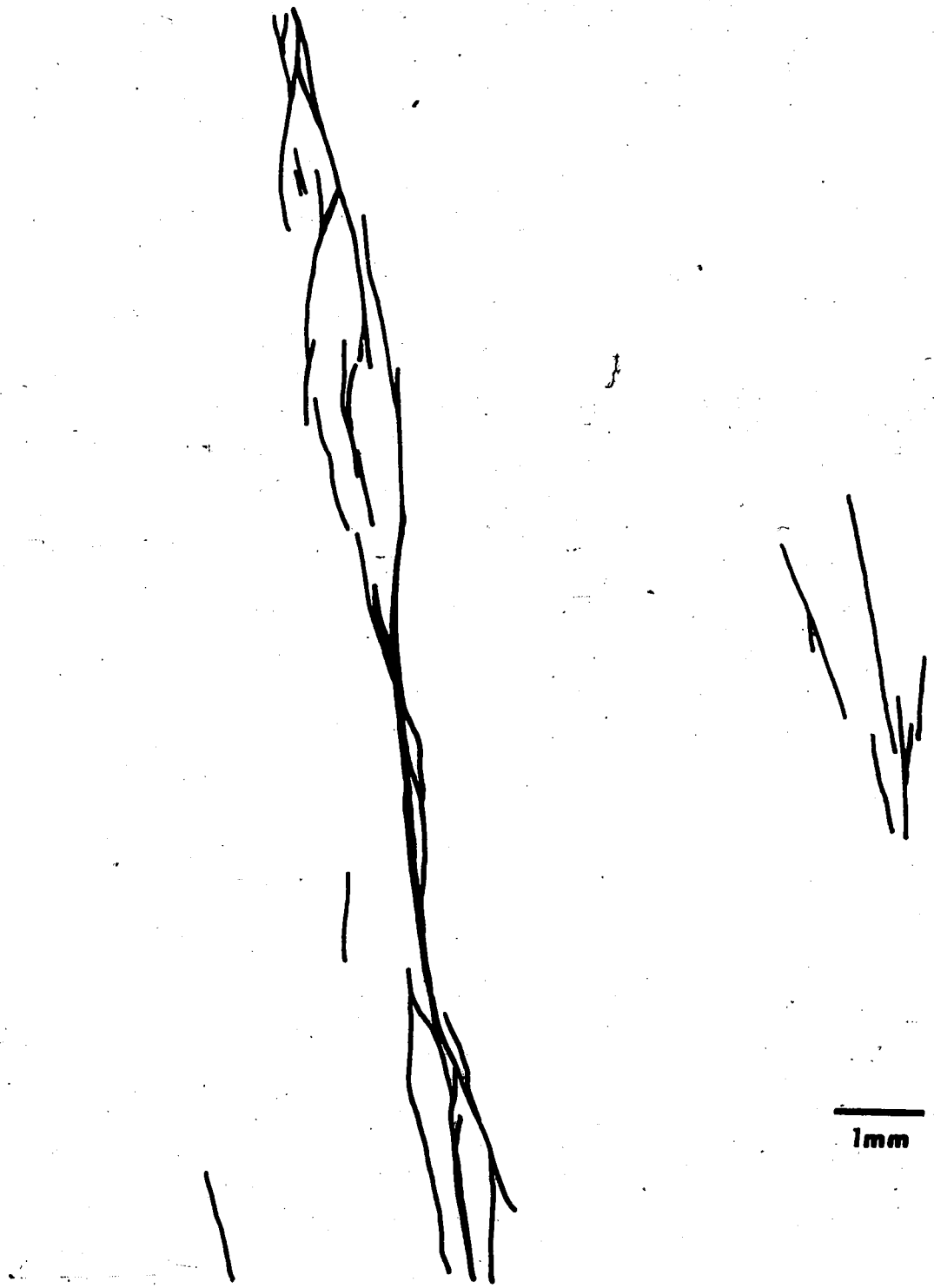

Figure 12: Tracing of Foliation from Thin Section of Sample 79-31.

(plate 22); at other times, it is barely discernable (plates 23, 24). The general condition within the folia seems to be somewhat chaotic-- zones are disrupted by silt particles (plate 24) and crossed or interupted by clays and micas with the bedding orientation (plates 25, 26, 27, 28).

The pole figure of 79-31 (fig. 13) reveals no contribution to x-ray intensity by the cleavage. The maximum pole density is 2.8, in the bedding plane. This is not surprising; the widest cleavage zone measured, 150 μm wide, accounts for only 1 percent of the volume irradiated by a 4 mm diameter beam.

DISCUSSION AND CONCLUSIONS

The pervasive shear fracturing in the experimentally deformed sediment is to be expected, considering the strain rate and the extremely low shear strength of the mud. (At higher strain rates, of course, mud with similarly high water contents would behave more plastically). More difficult to explain, however, are the crenulations. Several authors (Morganstern and Tchalenko, 1967; Tchalenko, 1968; Maltman, 1977) have suggested that crenulations in mud form in response to (horizontal) compression parallel to an initial preferred orientation formed by vertical consolidation. It might be asked, however, why crenulations form, rather than a simple unimodal

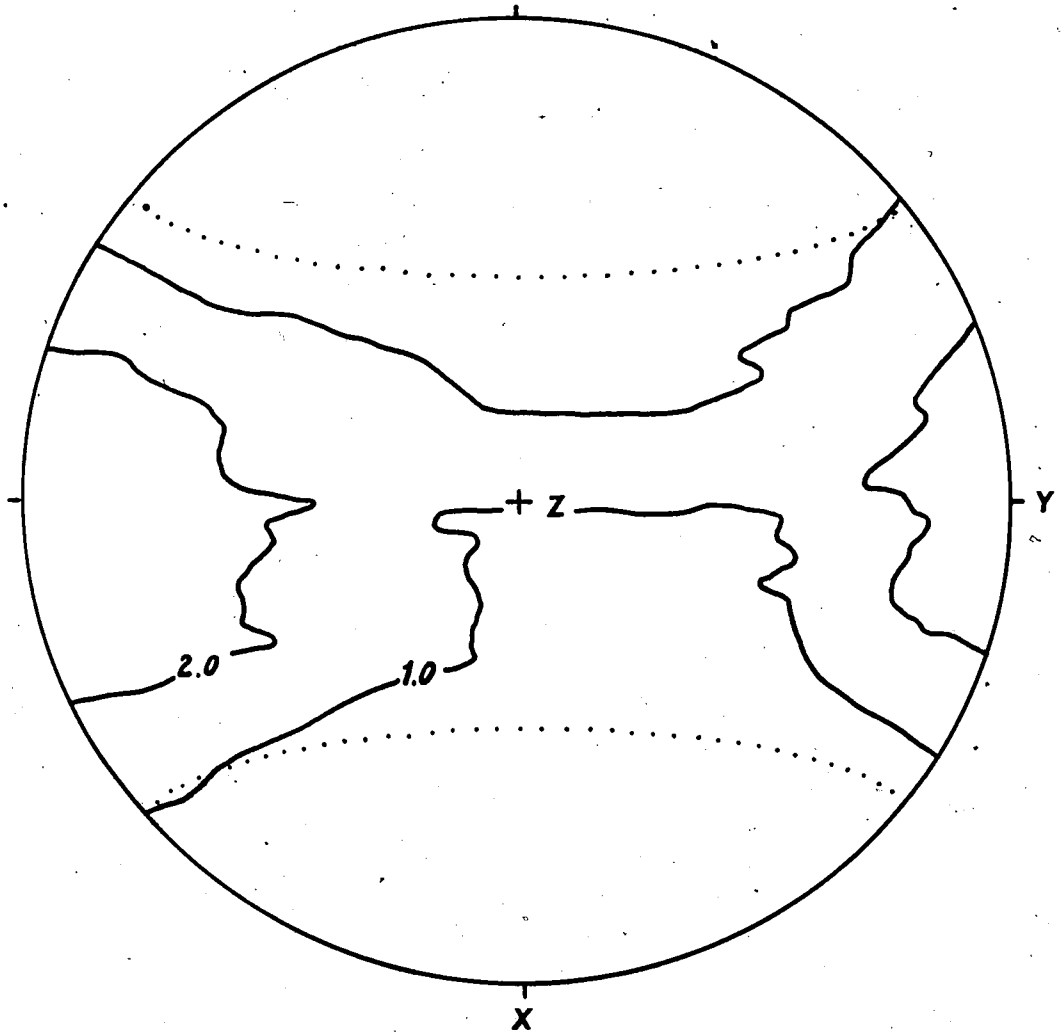

Figure 13: Partial Pole Figure for Sample 79-31.
Maximum Pole Density = 2.8.

rotation of flakes? The answer must lie in grain-to-grain interference (including interference by silt grains). The initial buckling of a pair of adjacent phyllosilicate flakes, perhaps facilitated by a slight initial angle between them, would encourage the same adjustment in surrounding flakes. Maltman (1977) has found that crenulations are part of a continuous sequence grading, with increasing strain, from kink bands, through crenulations, eventually to "creases", which he suggests may be genetically related to domainal slaty cleavage. At any rate, the crenulations, or more specifically the angles between the two preferred orientations which define each set, are presumably responsible for the smearing of most of the pole figure maxima (figs. 6, 7, 8, 9) into near-girdles.

In cases where what appear to be crenulations are observed at low angles to the z (longitudinal) axis of the squeezebox, the angles of alternate domains are always asymmetrical, and these structures are thought to be incipient shear fractures.

The strain history of the squeezebox is extremely complex. Geometrical limitations of the box itself have imposed a special pattern on the compressive stress field, and large amounts of translation and faulting, accompanied by some degree of rotational strain, have

together resulted in an extremely noncoaxial path of deformation. Preferred orientations which might have developed at one time and position in the box have, in all probability, been subjected to modification as that part of the mud mass is moved into a different area of the stress field. Furthermore, the strain history can be dealt with only qualitatively; the design of the experiment precludes strain determinations more accurate than estimates derived from water loss considerations.

If the direction of a preferred orientation is considered to be equivalent with that of the maximum finite shortening, it is evident from the pole figures and thin sections that that maximum strain has assumed widely differing orientations throughout the squeezebox. This is due mainly to boundary effects and the pervasive shear fracturing of the squeezebox mud.

In a squeezebox of infinite dimensions, the poles of the maximum finite shortening and resultant preferred orientation would be coincident with that of the axis of squeezing, the z axis. In a box of finite dimensions, however, as the mud is pushed forward by the plate, two simple shear systems are set up by that motion coupled with friction between the mud and the sides and bottom of the box. Each simple shear system, as shown in figure 14, results in its own maximum finite shortening,

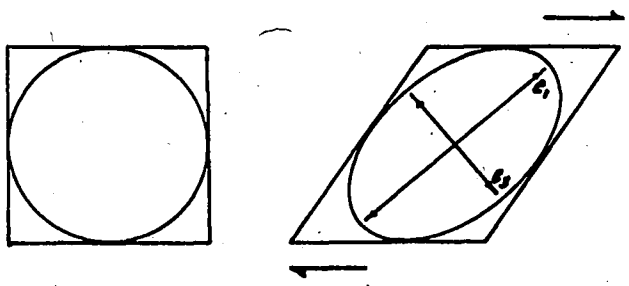

Figure 14: Compressional Strain Resulting from Simple Shear (after Ramsay, 1967, p 84). When the square is strained by simple shear, the internal circle becomes an ellipse; its major and minor axes indicate the maximum and minimum compressional strain axes. Clay flakes subject to such a system, such as those within a shear fracture zone, would tend to rotate parallel to the long axis of the ellipse.

which acts to modify the direction of the maximum finite shortening resulting directly from squeezing. The resulting vectors of maximum finite shortening would then follow the stress trajectories defined by Hafner (1951) for a system such as the squeezebox: coaxial with the z axis in the center of the mud, and elsewhere curving outward and downward toward the boundaries of the box.

Another, more local, source of shortening exists in the shear fracturing of the mud. Each thrust fault and shear fracture within the mud may be considered as a simple shear system, resulting in a maximum finite shortening between the upper and lower surface of the shear zone (figure 14). This shortening results in the alignment of clays at a small angle to the shear plane, as seen in plates 2, 3, 13, 14, and 17. The pole of the maximum finite shortening due to simple shear within thrust faults will lie between that of the z and x axes.

Shortening resulting directly from squeezing, as modified by boundary conditions, plus shortening components from shear fracturing, are summed together with any rotational strain, and the resultant is the direction of maximum finite shortening. The pole of the maximum finite shortening should then be the pole of the preferred orientation. Quantities are unknown for all of the components and thus for the resultant; only the relative importance

of each system at a given point can be inferred from the actual pole figures.

From water loss measured at various positions in the squeezebox, volume reductions can be calculated. These, in turn, yield strain estimates, which while revealing nothing of strain history, do furnish information on the distribution of total strain within the squeezebox. Assuming a specific gravity of 2.7 for the mud solids and 1.0229 for the Instant Ocean, the following volume reductions are derived:

Total volume loss = -9.2 percent

Volume loss at core position 5-1 = -13.2 percent

Volume loss at core position 5-2 = -13.6 percent

Volume loss at core position 5-4 = -6.6 percent

It is seen that most of the water loss and volume reduction has occured at the end nearest the plate, i.e., at the locus of deformation. If increase in the vertical dimension is neglected, the volume loss can be taken as the principal compressive strain at each location. In reality, however, the vertical dimension experienced considerable change: +28 percent at core position 5-1, +35 percent at core position 5-2, and no change at core position 5-4. If this change in height is considered to be extensional strain, the compressive strain (e_1) must become considerably larger to accomplish the volume

reductions calculated above:

Core position 5-1: e_1 = -32 percent

Core position 5-2: e_1 = -36 percent

Core position 5-4: e_1 = -6.6 percent

Thus, depending on whether the change in height is ignored or considered to be extensional strain, the estimates for e_1 assume minimum and maximum values.

It is evident, however, that much of the increase in the vertical dimension is the result of uplift by thrusting. If it is assumed that volume loss is accomplished strictly through horizontal compression, and the vertical increase is due entirely to faulting, the amount of displacement along thrust faults can be calculated for each location within the box:

At location 5-1, the 2.8 cm increase in height would require a 5.6 cm displacement along a 30° fault or a 8.7 cm displacement along a 20° fault (accounting for horizontal shortening of 4.85 and 7.7 cm respectively).

At location 5-2, the 3.5 cm increase in height would require a 7 cm displacement along a 30° fault or a 10.2 cm displacement along a 20° fault, accounting, respectively, for 6.1 and 9.6 cm of horizontal shortening.

The above considerations, together with the measured preferred orientation intensities, indicate that, while locations 5-1 and 5-2 have experienced essentially equal

volume loss, the dominant mode of strain differs at each location. At 5-1, there was less shear fracturing, and more horizontal compression, resulting in a higher degree of preferred orientation than at 5-2. This higher degree of preferred orientation was also accompanied by a higher vane shear strength (fig. 5), indicating strain hardening of the mud.

The predominance of horizontal compression over shear fracturing at location 5-1 is also indicated by the pole figures for that sample. The maximum for pole figure 5-1-3 (fig. 7) (yz plane) is coincident with that predicted for squeezing in the absence of any shearing. The maximum for 5-1-2 (fig. 6)(xz plane), while indicating the addition of a shear component, lies closer to the z axis than do the maxima of the pole figures for sample 5-2, again indicating that squeezing is dominant.

At location 5-2, shear fracturing dominated over horizontal compression, resulting in a lower degree of preferred orientation. Although water loss was actually greater at this position than at 5-1, vane shear strength was lower; strain hardening, then, apparently occurs more through development of preferred orientation than through simple water loss.

Both pole figures for sample 5-2 (figs. 8 and 9) have maxima that appear to have resulted from simple

shear between the mud and the side of the box, and simple shear caused by thrust faulting.

The data from sample 5-4 must be regarded with suspicion. It is unlikely that a volume loss of 6.6 percent would be accompanied by development of a higher degree of preferred orientation than that associated with a volume loss of 13.6 percent. Two possible sources of error exist for this sample that are negligable in the other two samples. First, the final water content of 5-4 was 15 percent greater than that of 5-1 and 18 percent greater than that of 5-2. This difference increases the likelihood that 5-4 may have been strained during the coring procedure. Second, the Carbowax impregnation of 5-4 was not as successful as that of 5-1 and 5-2 (see Methods), and the wax did not fully harden. This tended to make that specimen somewhat ductile, and additional strains may have been introduced during the preparation of x-ray transmission sections.

The differences in deformation at various locations within the box are largely a function of two variables: distance from the origin of the stress field (the plate), and time. The mud nearest the plate is deformed first; as preferred orientation begins to develop, water is presumably lost along the plane of the preferred orientation, between parallel phyllosilicate flakes. As deformation

proceeds, this mud becomes more coherent and eventually begins to behave as a rigid block, and is thrust over mud further from the plate. Deformation thus propagates away from the plate with time; the stresses in the more distant mud, however, are of smaller magnitude, having been attenuated largely by grain-to-grain friction. (At this greater distance from the plate, the orientation of the stress field also differs from that nearer the plate.) With less parallelism of phyllosilicate flakes, water loss at the more distant position may occur more along shear fracture planes, whose greater abundance at 5-2 (compared with 5-1) allow greater water loss despite a lower preferred orientation.

The strain distribution within the squeezebox, to a certain extent, models the real situation on the Northern Oregon-Washington lower continental slope. Structures and physical properties of sediments there have been interpreted as indicating a gradual seaward shift of the locus of deformation. Initial water loss occurs through horizontal compression, resulting in folding and strain hardening; when water content becomes low enough and sediment strength high enough, this stage is followed by overthrusting, and the development of a new fold further seaward (Carson et al, 1974; Carson, 1977).

Four possible mechanisms may be called upon to explain

development of the foliation observed in mudstone sample 79-31: shear fracturing, tension cracking, pressure solution and recrystallization, and veining due to dewatering. Comparison of high magnification photomicrographs of the cleavage with those of shear fractures of similar size in the squeezebox mud (plates 16 and 25) appears to rule out shear fracturing as a viable mechanism. In shear zones where phyllosilicates are aligned parallel to the shearing plane, this alignment is well defined and the individual flakes are very closely spaced. The alignment of phyllosilicates within the mudstone cleavage zones, however, is much more chaotic, and individual flakes are not as closely packed. Even in the widest cleavage folia, no preferred orientations were observed other than those parallel to the cleavage plane; in shear zones of equivalent width, preferred orientations are always at some angle to the shear plane.

Tension fractures are readily dismissed as a mechanism here for two reasons: First, the cleavage folia do not exhibit any gaps or openings, however small, such as would be expected to occur under tension. Second, tension would be accompanied by orthogonal compression, which would result in a preferred orientation normal to the plane of the tension crack, which is not observed.

No crystallographic or morphological evidence (e.g.,

truncated quartz grains) has been observed that would support the existence of pressure solution in this mudstone. Physical properties essentially rule out this possibility; the high water content (~30 percent) as well as seismic profiles (Carson et al, 1974) indicate that burial of these deposits has been negligable (≤60m).

While sufficient pressure for initiation of pressure solution might have been supplied by the offscraping and accretion process, the necessary source of heat is lacking. Furthermore, the mudstone contains numerous foraminifera and diatom tests which are completely undeformed; any pressure solution activity would certainly result in partial dissolution of at least the carbonate tests.

There remains but one reasonable mechanism, then, for development of this cleavage: dewatering. The mechanism proposed here is not the escape of pore fluid permitted by rotation of phyllosilicate grains, but rather the converse. Were the former mechanism operational here, there would be no reason to expect the occurrence of preferred orientations only in discrete planes. In several cases, phyllosilicates are observed along the borders of cleavage folia in orientations intermediate to those of bedding and cleavage (plates 23 and 29), suggesting the passage of pore fluids from surrounding beds into the mainstream of escaping pore fluid. The process may

be essentially instantaneous (as suggested by the sometimes chaotic nature of the preferred orientation within the individual folia). When pore fluid pressure exceeds the strength of the sediment, the fluid apparently escapes along the plane of the intermediate and minor stress axes.

It is conceivable that, at greater depths of burial and thus greater confining pressures, fluid escape might be prevented (or postponed), allowing attainment of much higher pore pressures. In this manner, pore pressures high enough to allow a more pervasive rotation of phyllosilicates might be reached.

The amount of strain experienced by mudstone 79-31 can only be estimated. Carson et al (1974) calculated (by fold geometry considerations) a maximum of two percent shortening on a single ridge. The water content of the mudstone (~30 percent), however, indicates that considerable volume reduction has occured since initial deposition. A minimum loss in volume may be calculated in the following manner, assuming an initial water content of 50 percent prior to offscraping and accretion, and specific gravities of 1.03 for sea water and 2.7 for the solid constituents of the mudstone:

wc = water content (percent dry weight)
vt = total volume
vs = volume of solids
vw = volume of water

wc (initial) = 0.50

$\frac{vw}{vs} = wc \cdot \frac{\text{sp.gr. solids}}{\text{sp.gr. water}} = (0.50)\frac{(2.7)}{(1.03)} = 1.31$

vt = vs + vw

vw = 1.31vs

vt = 2.31vs

for unit volume, vs = 0.433
vw = 0.567

after offscraping and accretion,

wc = 0.30
vs = 0.433 (no change)

$\frac{vw}{vs} = wc \cdot \frac{\text{sp.gr. solids}}{\text{sp.gr. water}} = 0.786$

vw = 0.786vs = (0.786)(0.433)

vt = 0.774

volume reduction = 23 percent.

Assuming negligable dimensional changes in the two directions perpendicular to the principal compressive strain axis, the calculated volume reduction is accomplished by a compressive strain of -0.23. This value would increase with greater initial water content, and decrease with the addition of strains on the other axes. It is somewhat larger than the principal compressive strains estimated for the deformed portion of the squeeze-box mud (-0.13), and considerably smaller than the mean principal compressive strain, -0.70, given by Wood (1974) for over 5000 slates. Without knowledge of the initial

water content of the mudstone, however, the comparison of this strain estimate with that for the squeezebox loses some significance. Still more caution must be exercised in comparing it to strain measurements in slates; reduction spots, the most common source of strain measurements for slates, are diagenetic features; any strain experienced prior to the time of their development in a sediment is not included in the final measurement. The mudstone in question, then, has not necessarily undergone a third of the total compressive strain measured in most slates.

While the overall scheme of deformation is grossly similar in each case, structures similar to the mudstone cleavage are not observed in the squeezebox mud. This may be due in part to the pervasive nature of shear fracturing in the squeezebox. These fractures provide ready channels for drainage of pore fluids, and apparently prevent the attainment of abnormal pore pressures required for rapid fluid escape. Preferred orientations in the squeezebox presumably form by wholesale rotation, but are always of limited volumetric extent.

In conclusion, it has been shown that rudimentary spaced cleavage may develop through dewatering of deep sea sediments in response to off-scraping and accretion to the continental margin. This cleavage has apparently developed during escape of overpressured pore fluid.

Furthermore, preferred orientations have been artificially induced in similar sediments during dewatering. These experimentally induced preferred orientations presumably have occured by means of wholesale rotation of phyllosilicates, rather than by sudden escape of pore fluid.

It is not proposed here that slaty cleavage ultimately develops strictly as the result of dewatering, but it is clear that incipient "soft sediment" deformation leads to phyllosilicate reorientation in spaced folia. The development of phyllosilicate preferred orientation and thus slaty cleavage must be looked upon as a continuum, with soft-sediment processes dominant at one end and solid state processes at the other. It has been shown that incipient preferred orientations, however weak, can develop in response to dewatering. Once formed, such initial anisotropies may be subject to later enhancement by higher level processes, perhaps resulting, in the end, in the formation of true slaty cleavage.

REFERENCES

Alterman, I.B., 1973, Rotation and dewatering during slaty cleavage formation: some new evidence and interpretations: Geology, v. 1, p. 33-36.

_____, 1976, Slaty cleavage and the dewatering hypothesis: an examination of some critical evidence: comment: Geology, v. 4, p. 789-790.

Atwater, T., 1970, Implications of plate tectonics for the Cenozoic tectonics of western North America: Geol. Soc. Am. Bull., v. 81, p. 3513-3536.

Baker, D.W., Wenk, H.R., and Christie, J.M., 1969, X-ray analysis of preferred orientation in fine grain quartz aggregates: Jour. Geol. v. 77, p. 144-172.

Barnes, W.C., and Ross, J.V., 1973, Buckle folding, thrust faulting, and mineral orientation associated with dewatering of Pleistocene lake sediments (abs): Geol. Soc. Am. Abs., v. 5, p. 7.

Barret, C.S., and Massalski, T.B., 1966, Structure of metals (3rd Ed.): New York, McGraw-Hill Book Co., 654p.

Boulter, C.A., 1974, Tectonic deformation of soft sedimentary clastic dikes from the Precambrian rocks of Tasmania, Australia, with particular reference to their relations with cleavages: Geol. Soc. Am. Bull., v 85, p. 1413-1420.

Braddock, W.A., 1970, The origin of slaty cleavage: evidence from Precambrian rocks in Colorado: Geol. Soc. Am. Bull., v 81, p. 589-600.

Burger, H.R., 1974, Pressure-solution: how important a role (abs): Geol. Soc. Am. Abs., v. 6, p. 1026-1027.

Carson, B., 1976, Deformation of deep-sea sediments off Washington and northern Oregon: Mechanical consolidation: Marine Geol., v. 24, p. 289-307.

Carson, B., Yuan, J., Myers, P.B., Jr, Barnard, W.D., 1974, Initial deep-sea sediment deformation at the base of the Washington continental slope: a response to subduction: Geology, v. 2, p. 561-564.

Carson, W., 1968, Development of flow cleavage in the Martinsburg shale, Port Jervis South area (northern New Jersey): Tectonophysics, v. 5, p. 531-541.

Chawla, K.S., 1973, Effect of fabric on creep response of kaolinite clay: Ph.D. Thesis, Northwestern University, 165p.

Clark, B.R., 1970a, Origin of slaty cleavage in the Coeur d'Alene district, Idaho: Geol. Soc. Am. Bull., v. 81, p. 3061-3072.

_____, 1970b, Mechanical formation of preferred orientation in clays: Am. Jour. Sci., v. 269, p. 250-266.

Cloos, E., 1947, Oölite deformation in the South Mountain fold, Maryland: Geol. Soc. Am. Bull., v. 58, p. 843-918.

Decker, B.F., Asp, E.T., and Harker, D., 1948, Preferred Orientation determination using a Geiger counter x-ray diffraction goniometer: Jour. Appl. Physics, v. 19, p. 388-392.

Durney, D.W., 1972, Solution-transfer, an important geological deformation mechanism: Nature, v. 235:5337, p. 315-317.

Geiser, P.A., 1975, Slaty cleavage and the dewatering hypothesis- and examination of some critical evidence: Geology, v. 3, p. 717-720.

_____, 1974, Cleavage in some sedimentary rocks of the Central Valley and Ridge Province, Maryland: Geol. Soc. Am. Bull., v. 85, p. 1399-1412.

Gillot, J.E., 1970, Fabric of Leda clay investigated by optical, electron-optical, and x-ray diffraction methods: Eng. Geol., v. 4, p. 133-153.

Groshong, R.H., Jr., 1975, "Slip" cleavage caused by pressure solution in a buckle fold: Geology, v. 3, p. 411-413.

_____, 1976, Strain and pressure solution in the Martinsburg slate, Delaware Water Gap, New Jersey: Am. Jour. Sci., v. 276, p. 1131-1146.

Holeywell, R.C., and Tullis, T.E., 1975, Mineral reorientation and slaty cleavage in the Martinsburg formation, Lehigh Gap, Pennsylvania: Geol. Soc. Am. Bull., v. 86, p. 1296-1304.

Kazi, A., 1975, Quantitative fabric analysis of Drammen clay using x-ray diffraction technique: Jour. Sed. Pet., v. 45, p. 883-890.

Lipshie, S.R., Oertel, G., and Christie, J.M., 1976, Measurement of preferred orientation of phyllosilicates in schists: Tectonophysics, v. 34, p. 91-99.

Maltman, A.J., 1977, Some microstructures of experimentally deformed argillaceous sediments: Tectonophysics, v. 39, p. 417-436.

Martin, R.T., 1966, Quantitative fabric of wet kaolinite: Clays and Clay Minerals, Proceedings of 14th National Conference, Berkley, California, p. 271-287.

Maxwell, J.C., 1962, Origin of slaty and fracture cleavage: Petrologic Studies (Buddington volume), New York, Geol. Soc. Am., p. 281-310.

_____, 1976, Slaty cleavage and the dewatering hypothesis: an examination of some critical evidence: comment: Geology, v. 4, p. 790-791.

Means, W.D., and Patterson, M.S., 1966, Experiments on preferred orientation of platy minerals: Contr. to Min. and Petr., v. 13, p. 108-133.

Mitchell, J.K., 1956, The fabric of natural clays and its relation to engineering properties: Proceedings of 35th Annual Meeting, Highway Research Board, Washington, D.C., p. 693-713.

Moench, R.H., 1966, Relation of S_2 schistosity to metamorphosed clastic dikes, Rangeley-Phillips area, Maine: Geol. Soc. Am. Bull., v. 77, p. 1449-1462.

_____, 1970, Premetamorphic down-to-basin faulting, folding, and tectonic dewatering, Rangeley Area, Western Maine: Geol. Soc. Am. Bull., v. 81, p. 1463-1496.

Moore, J.C., 1973, Complex deformation of Cretaceous trench deposits, southwestern Alaska: Geol. Soc. Am. Bull., v. 84, p. 2005-2020.

Moore, J.C., and Geigle, J.E., 1974, Slaty cleavage: incipient occurences in the deep sea: Science, v. 183, p. 509-510.

Morganstern, N.R., and Tchalenko, J.S., 1967, Microscopic structures in kaolin subjected to direct shear: Geotechnique, v. 17, p. 309-328.

Myers, P.V., van Sciver, W.J., and Richards, A.F., 1974, Theory of nuclear transmission densitomrtry applied to sedimentology and geotechnology, Jour. Sed. Petr., v. 44, p. 1010-1015.

Oertel, G., 1970, Deformation of a slaty, lapillar tuff in the Lake District, England: Geol. Soc. Am. Bull., v. 81, p. 1173-1188.

Oertel, G., and Curtis, C.D., 1972, Clay-ironstone concretion preserving fabrics due to progressive compaction: Geol. Soc. Am. Bull., v. 83, p. 2597-2606.

Powell, C.McA., 1969, Intrusive sandstone dykes in the Siamo Slate near Negaunee, Michigan: Geol. Soc. Am. Bull., v. 80, p. 2585-2594.

_____, 1972a, Tectonically dewatered slates in the Ludlovian of the Lake District, England: Geol. Jour., v. 8, p. 95-110.

_____, 1972b, Tectonic dewatering and strain in the Michigamme Slate, Michigan: Geol. Soc. Am. Bull., v. 83, p.2149-2158.

_____, 1973, Clastic dikes in the Bull formation of Cambrian age, Taconic allochthon, Vermont: Geol. Soc. Am. Bull., v. 84, p. 3045-3050.

_____, 1974, Timing of slaty leavage during folding of Precambrian rocks, northeast Tasmania: Geol. Soc. Am. Bull., v. 85, p. 1043-1060.

_____, 1976, Slaty cleavage and the dewatering hypothesis: an examination of some critical evidence: comment: Geology, v. 4, p. 792.

Quigley, R.M., and Thompson, C.D., 1966, The fabric of anisotropically consolidated sensitive marine clay: Canadian Geotechnical Jour., v. 3, p. 61-73.

Ramsay, J.G., 1967, Folding and Fracturing of Rocks: New York, McGraw-Hill, 568 p.

_____, 1976, Displacement and strain: Phil Trans. R. Soc. London, ser. A, v. 283, p. 3-25.

Ramsay, J.G., and Wood, D.S., 1973, The geometric effects of volume change during deformation processes: Tectonophysics, v. 16, p. 263-277.

Richards, A.F., Hirst, T.J., and Parks, J.M., 1974, Bulk density -water content relationship in marine silts and clays: Jour. Sed. Petr., v. 44, p. 1004-1009.

Rubey, W.W., and Hubbert, M.K., 1959, Role of fluid pressure in the mechanics of overthrust faulting II, Overthrust belt of geosynclinal area of western Wyoming in light of fluid-pressure hypothesis: Geol. Soc. Am. Bull., v. 70, p. 115-206.

Siddans, A.W.B., 1972, Slaty cleavage- a review of research since 1815: Earth Science Reviews, v. 8, p. 205-232.

_____, 1976, Deformed rocks and their textures: Phil. Trans. R. Soc. Lond., Ser. A, v. 283, p. 43-54.

_____, 1977, The development of slaty cleavage in a part of the French Alps: Tectonophysics, v. 39, p. 533-557.

Silver, E.A., 1972, Pleistocene tectonic accretion of the continental slope off Washington: Marine Geol., v. 13, p. 239-250.

Tchalenko, J.S., 1968, The evaluation of kink bands and the development of compression textures in sheared clays: Tectonophysics, v. 6, p. 159-174.

Tchalenko, J.S., Burnett, A.D., and Hung, J.J., 1971, The correspondence between optical and x-ray measurements of particle orientation in clays: Clay Minerals, v. 9, p. 47-70.

Tullis, T., 1971, Experimental development of preferred orientation of mica during recrystallization (Ph.D. thesis): Ann Arbor, Michigan, University Microfilms, 262 p.

Tullis, T.E., and Wood, D.E., 1975, Correlation of finite strain from both reduction bodies and preferred orientation of mica in slate from Wales: Geol. Soc. Am. Bull., v. 86, p. 632-638.

von Huene, R., and Kulm, L.D., 1973, Tectonic summary of Leg 18, Initial Reports of the Deep Sea Drilling Project, v. 18, p. 961-976.

Williams, P.F., 1972, Development of metamorphic layering and cleavage in low-grade metamorphic rocks at Bermagui, Australia: Am. Jour. Sci., v. 262, p. 1-47.

Williams, P.F., 1976, Relationships between axial-plane foliations and strain: Tectonophysics, v. 30, p. 181-196.

Wood, D.S., 1974, Current views of the development of slaty cleavage: Ann. Rev. Earth and Plan. Sci., v. 2, p. 369-401.

Wood, D.S., Oertel, G., Singh, J., and Bennett, H.F., 1976, Strain and anisotropy in rocks: Phil. Trans. R. Soc. Lond., ser. A, v. 283, p. 27-42.

Plate 1: Specimen 5-1, xz plane; crossed nichols, gypsum plate; photographed in red light to enhance contrast. Two shear fractures inclined 40° and 50° to z. Platelets in surrounding and interlying areas are generally oriented perpendicular to shear fractures. Note, however, crenulations in lower right quarter of plate. These crenulations trend about 15° from the x axis; clay flakes in one set are parallel to shear fractures, those in alternate set perpendicular. White area in top of plate is Carbowax; note set of small shear fractures to left. Objective 3.5x.

Plate 2: Specimen 5-1, xz plane; crossed nichols, gypsum plate, red light. View of two shear zones (dark areas) trending 25° to 30° clockwise from z. Platelets within shear zones are oriented 50° clockwise from z. Area between shear zones consists largely of very narrow (25μm) shear dislocations inclined 40° counterclockwise from z. Objective 10x.

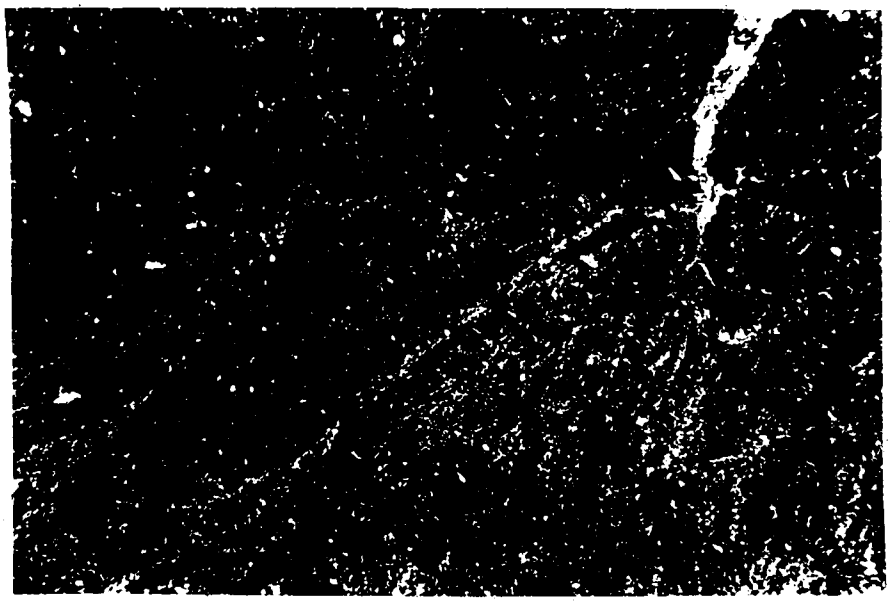

PLATE 1

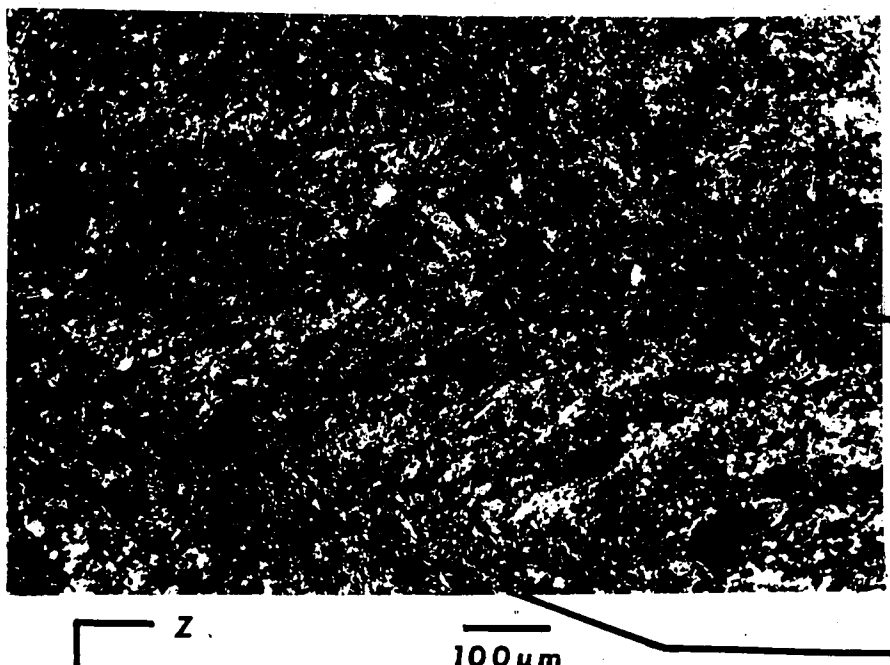

PLATE 2

Plate 3: Specimen 5-2, xz plane; crossed nichols, gypsum plate, red light. View of shear zone, inclined 25° clockwise from z (in this photograph z is parallel to the short side). Clay flakes within shear zone are oriented 40° clockwise from z. Clays surrounding shear zone lie at 35° to 45° counterclockwise from z. Note conjugate set of smaller shear fractures at left. Objective 10x.

Plate 4: Specimen 5-2, yz plane; crossed nichols, gypsum plate, red light. Preferred orientation, possibly that due to horizontal compression, 15° clockwise from the y axis, shown also by elongate silts. Shear zones subparallel with z axis, and flakes within are oriented 30° clockwise from z. Objective 10x.

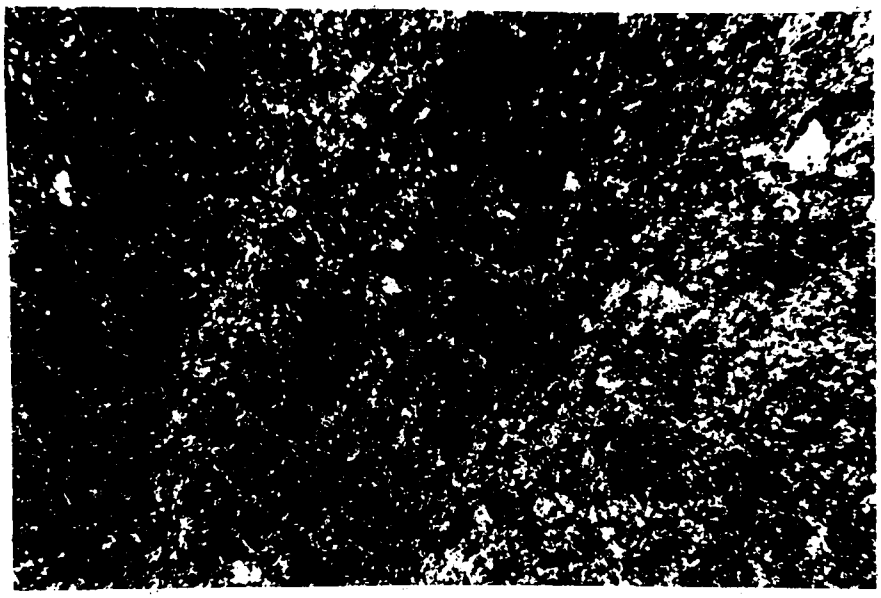

PLATE 3

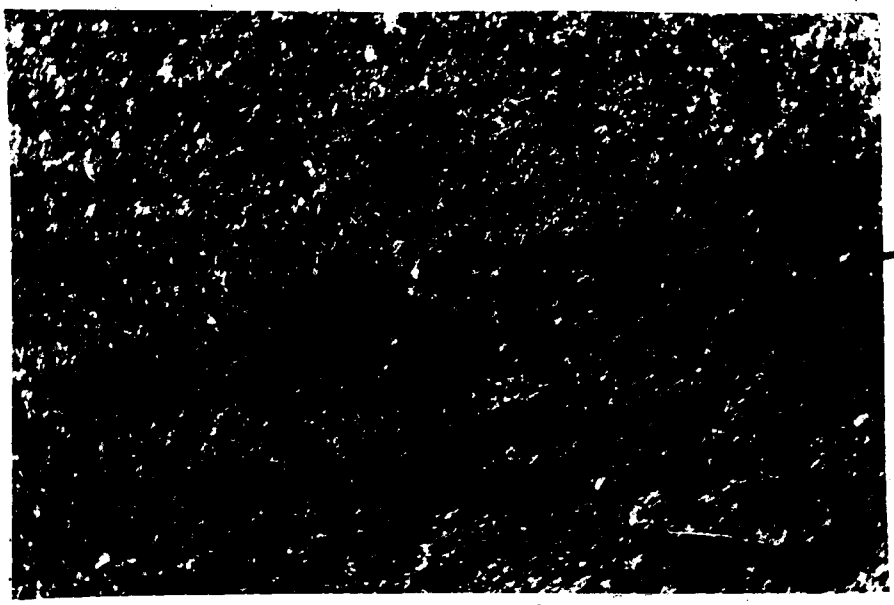

PLATE 4

Plate 5: Specimen 5-1, xz plane; crossed nichols, gypsum plate, red light. View of crenulations. Flakes in light areas are oriented 50° counterclockwise from z; those in darker areas lie 50° clockwise from z. Objective 10x.

Plate 6: Specimen 5-1, yz plane; crossed nichols, gypsum plate, red light. View of crenulations, which trend parallel to y axis. Axial angle formed is 60°. Objective 10x.

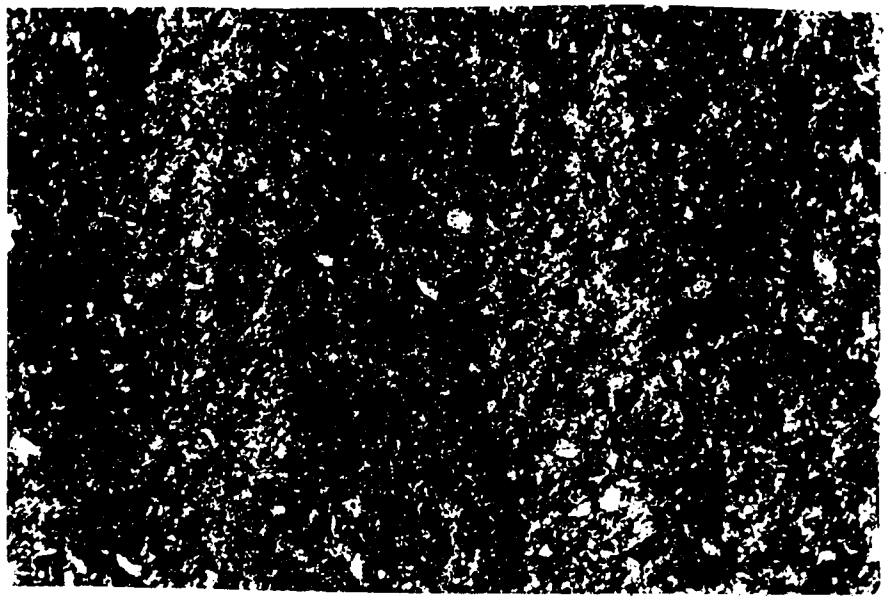

Z

X

100μm

PLATE 5

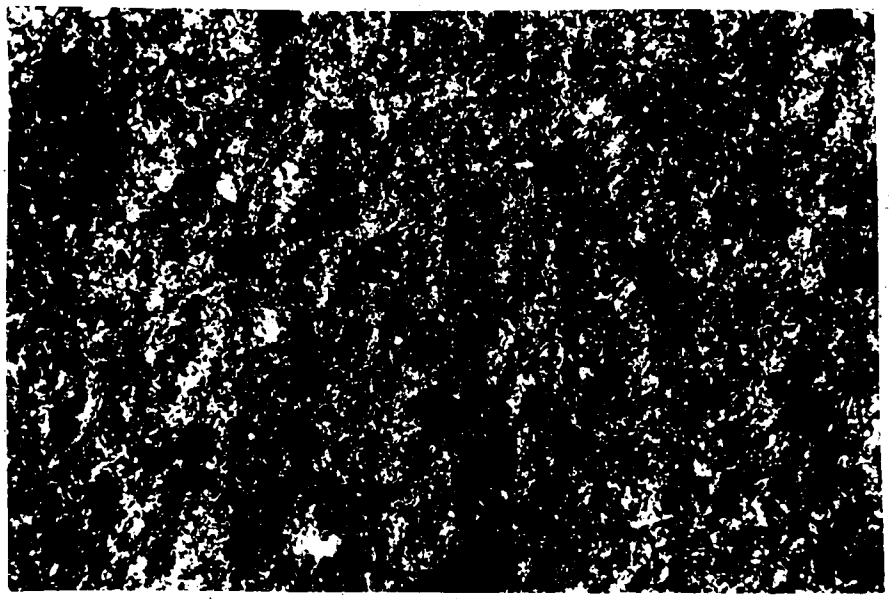

Z

Y

100μm

PLATE 6

Plate 7: Specimen 5-1, yz plane; crossed nichols, gypsum plate, red light. Crenulations, axial angle 90°. Objective 25x.

Plate 8: Specimen 5-2, xz plane; crossed nichols, gypsum plate, red light. Dominant orientation is 50° to 60° clockwise from z, with a few crenulations with opposite attitude. Objective 10x.

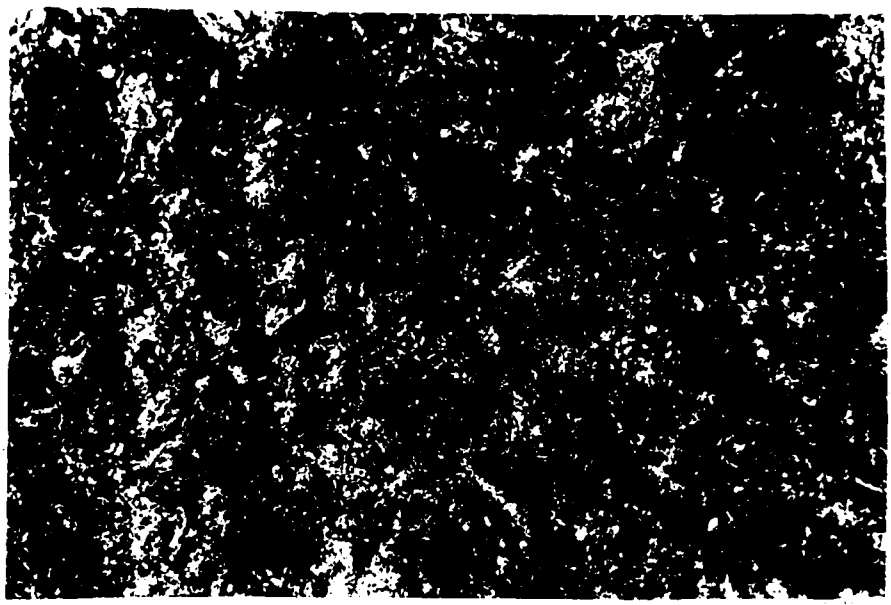

PLATE 7

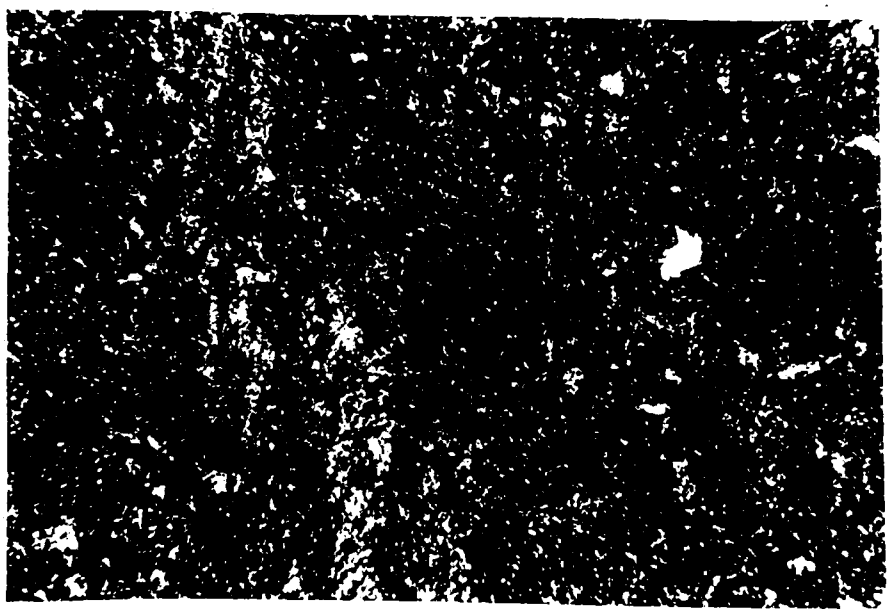

PLATE 8

Plate 9: Specimen 5-2, xz plane; crossed nichols, gypsum plate, red light. View of crenulations from plate 8. Objective 95x oil immersion.

Plate 10: Specimen 5-2, xz plane, crossed nichols, gypsum plate, red light. Crenulations, with axial angle of 100°. Objective 10x.

Z

X

10μm

PLATE 9

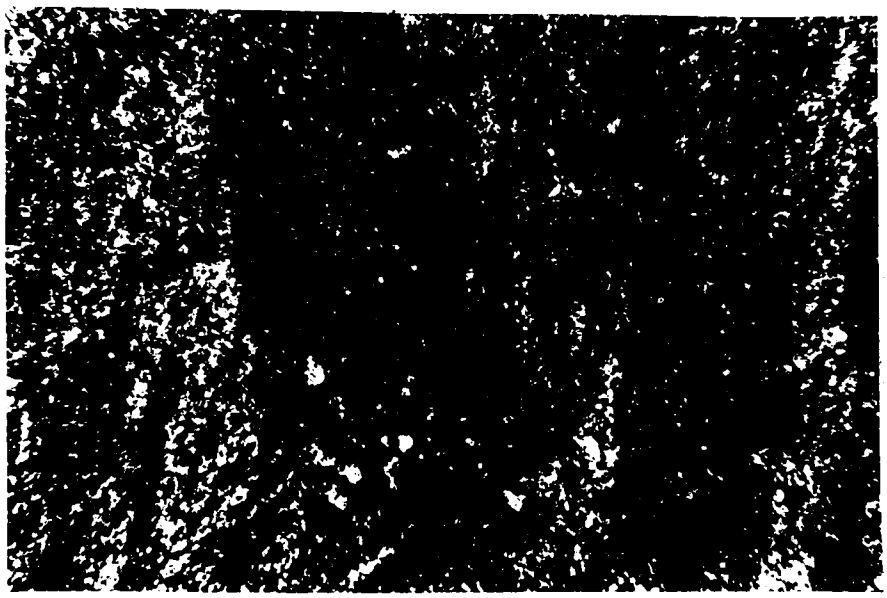

Z

X

100μm

PLATE 10

Plate 11: Specimen 5-2, xz plane; crossed nichols, gypsum plate, red light. Crenulations with axial angle of 80°. Objective 10x.

Plate 12: Specimen 5-2, yz plane; crossed nichols, gypsum plate, red light. Crenulations with axial angle of 80°. Objective 50x.

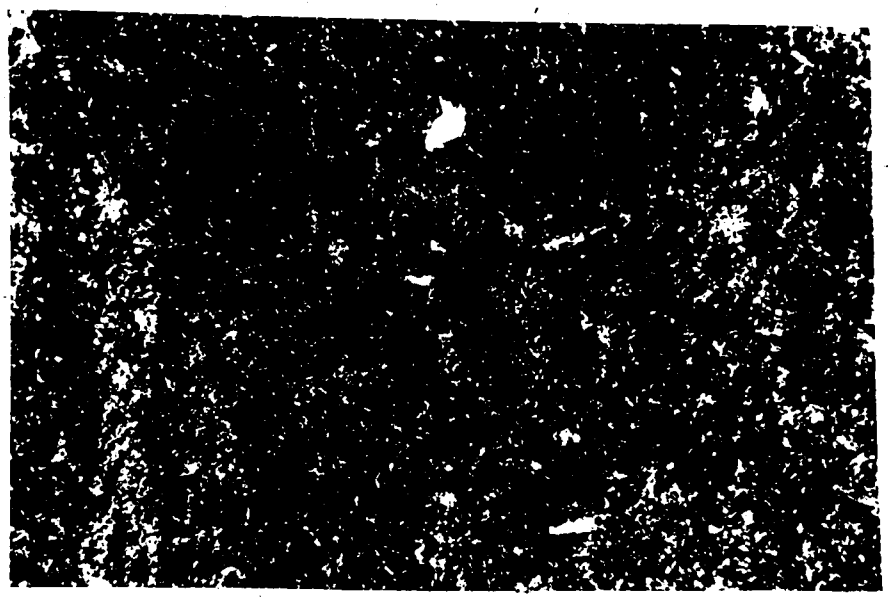

Z

X

100μm

PLATE 11

CRENULATION AXIS

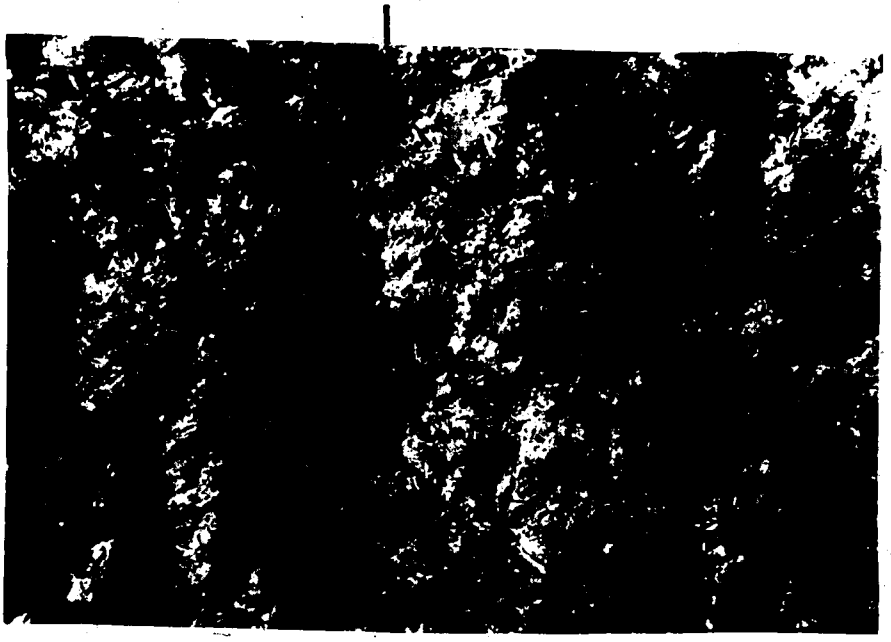

Z

Y

100μm

PLATE 12

Plate 13: Specimen 5-2, xz plane, crossed nichols, gypsum plate, red light. Fault gouge of macro-fault. Orientation of surrounding area trends 45° counterclockwise from z; some flakes in center of "fault zone" maintain this orientation; majority of clays within gouge, however, lie parallel to direction of displacement. Objective 3.5x.

Plate 14: Specimen 5-1, xz plane; crossed nichols, gypsum plate, red light. Shear zone across bottom of photograph, inclined 5° counterclockwise to z axis. Clay flakes within shear zone are well aligned at 30° clockwise from z, indicating sinestral displacement. Above shear zone, flakes are dominantly oriented 45° counterclockwise from z, with narrow domains following the same orientation wherin platelets are oriented 85° counterclockwise from z. These domains are more apparent in plate 11. Objective 10x.

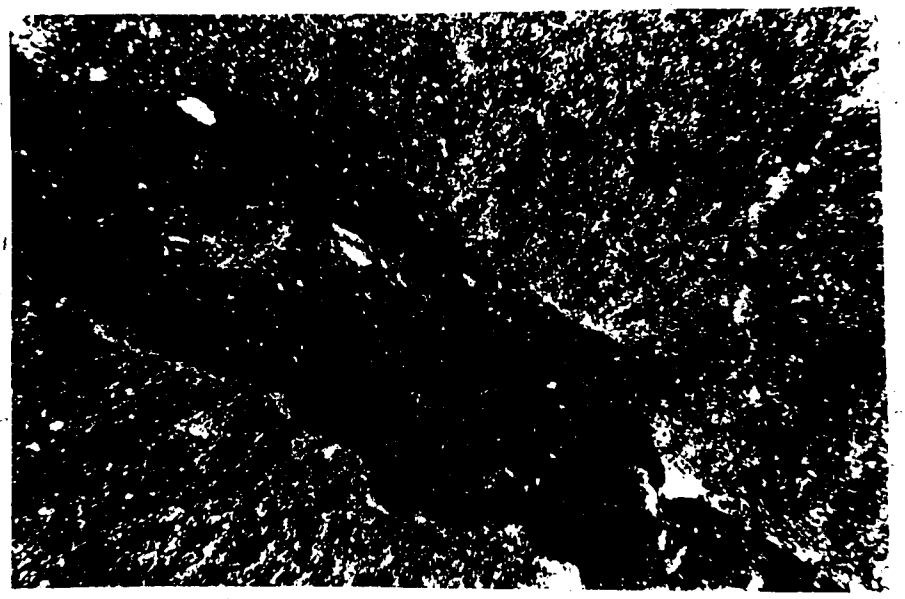

PLATE 13

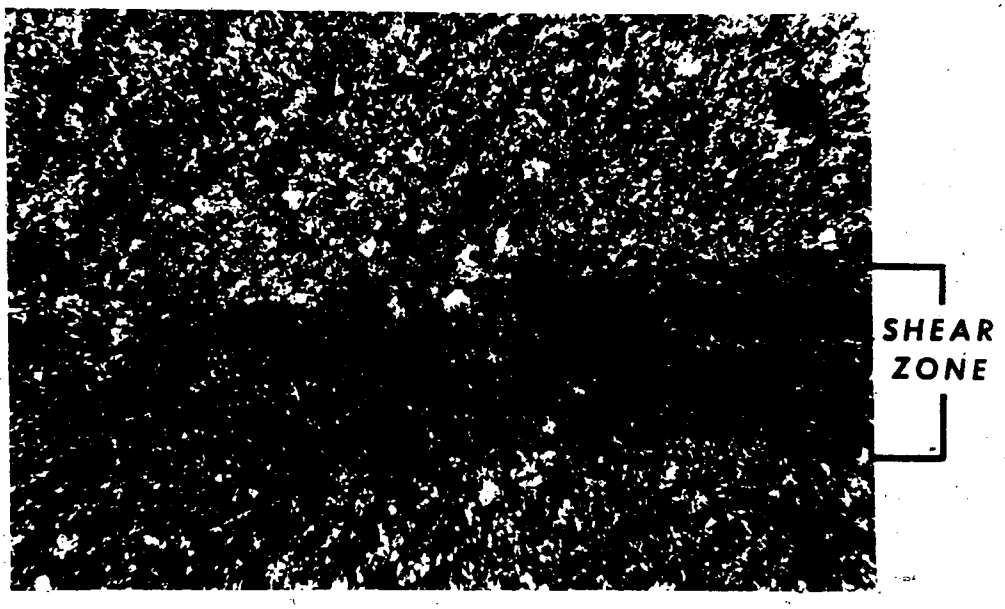

PLATE 14

Plate 15: Enlarged view of center of plate 1. Specimen 5-1, xz plane; crossed nichols, gypsum plate, red light. Shear fracture (light area) inclined 40° to z. Platelets in surroundeing area are generally oriented perpendicular to shear fracture. Objective 10x.

Plate 16: Specimen 5-1, xz plane; crossed nichols, gypsum plate, red light. High magnification view of shear plane of the type shown in plates 1 and 15. Note well developed parallelism to shear plane. Objective 95x oil immersion.

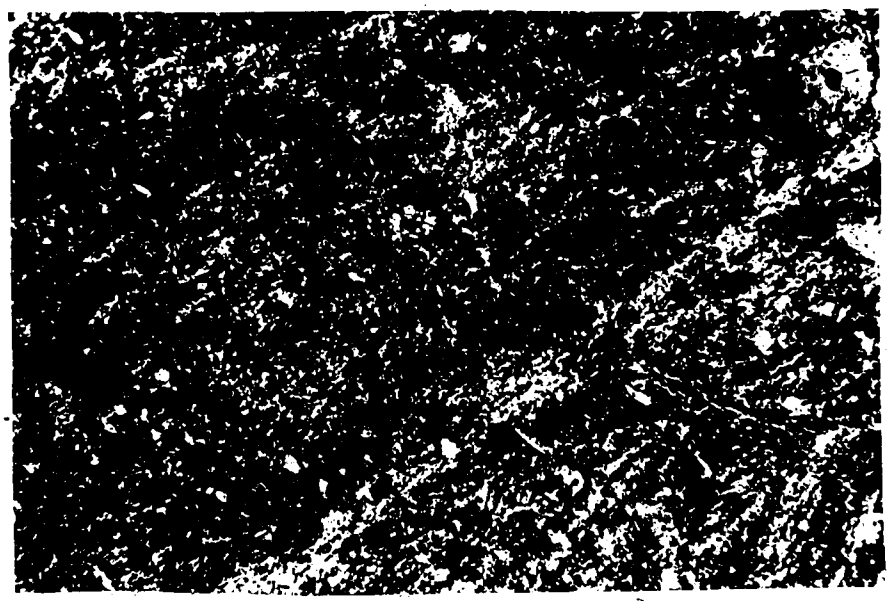

Z

X

100μm

PLATE 15

SHEAR ZONE

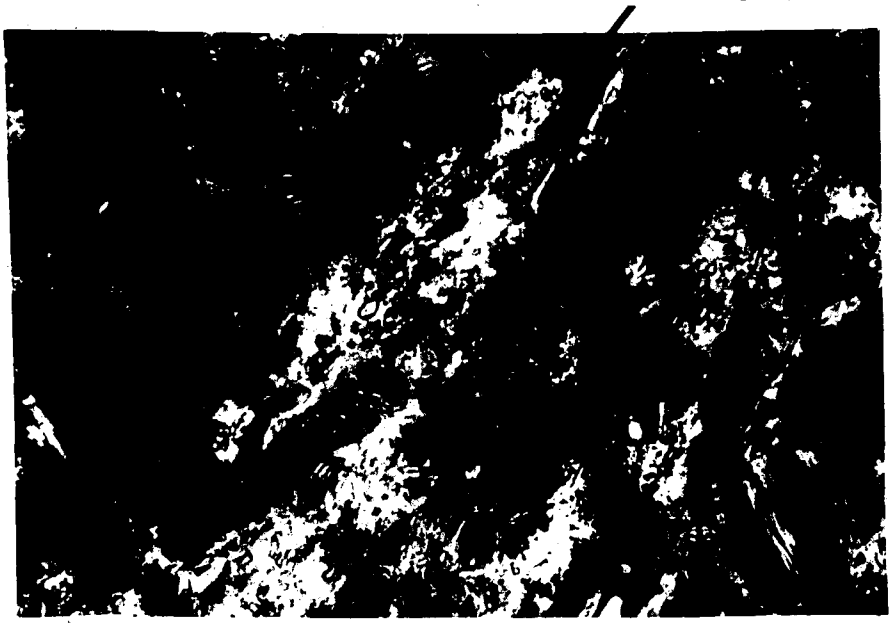

Z

X

10μm

PLATE 16

Plate 17: Specimen 5-1, xz plane; crossed nichols, gypsum plate, red light. Same field as plate 10, rotated 30^{o} counterclockwise. Note narrow plane of clays oriented parallel to shear displacement (running diagonally lower left to upper right). Domainal structure also more apparent in upper left portion of photograph. Objective 10x.

Plate 18: Specimen 5-1, xz plane; crossed nichols, gypsum plate, red light. "Expected" preferred orientation, striking parallel with the x axis, i.e., 45^{o} from the horizontal. Orientation is not uniform; fabric consists of narrow domains in which the platelets make a small angle ($\leq 5^{o}$) with the x axis; in adjacent domains the sense of the angle is opposite. Objective 10x.

SHEAR ZONE

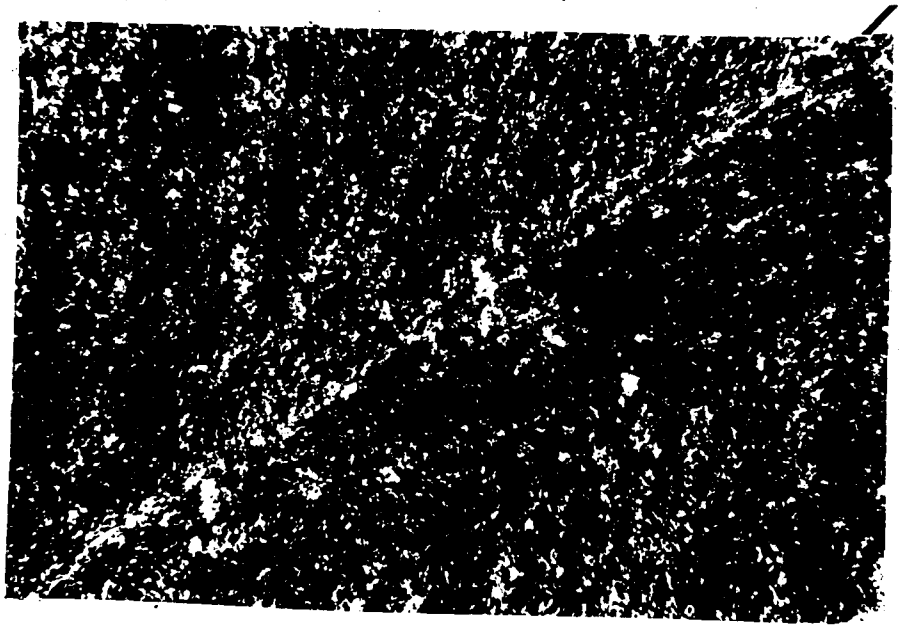

Z
X

100μm

PLATE 17

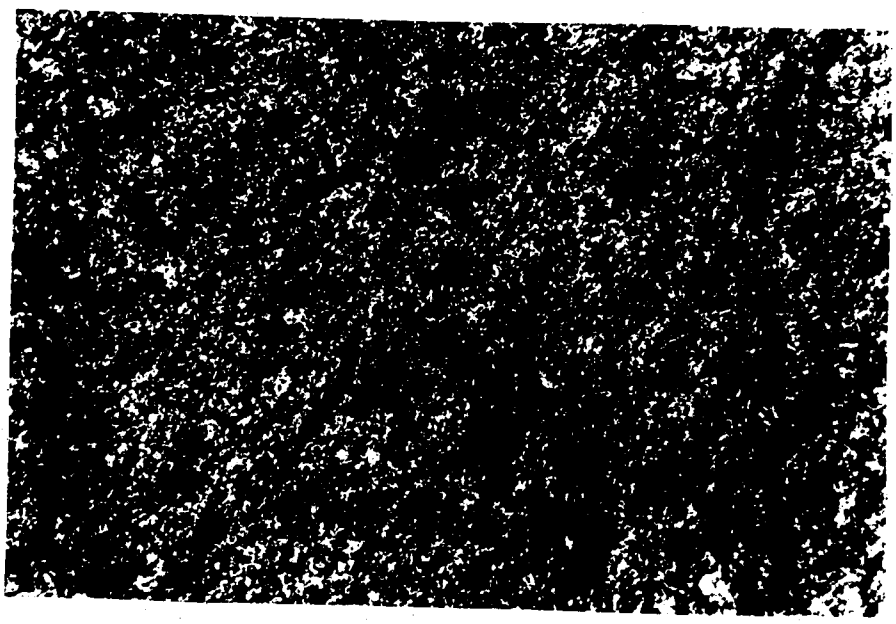

100μm

X
Z

PLATE 18

Plate 19: Specimen 5-2, yz plane; crossed nichols, gypsum plate, red light. Preferred orientation, probably that due directly to horizontal compression, running parallel to the y axis. Shown by elongate silts as well as clays. Objective 10x.

Plate 20: Specimen 79-28; crossed nichols, gypsum plate. Section normal to bedding/cleavage. Bedding trends NE-SW. Note well developed preferred orientation. Objective 10x.

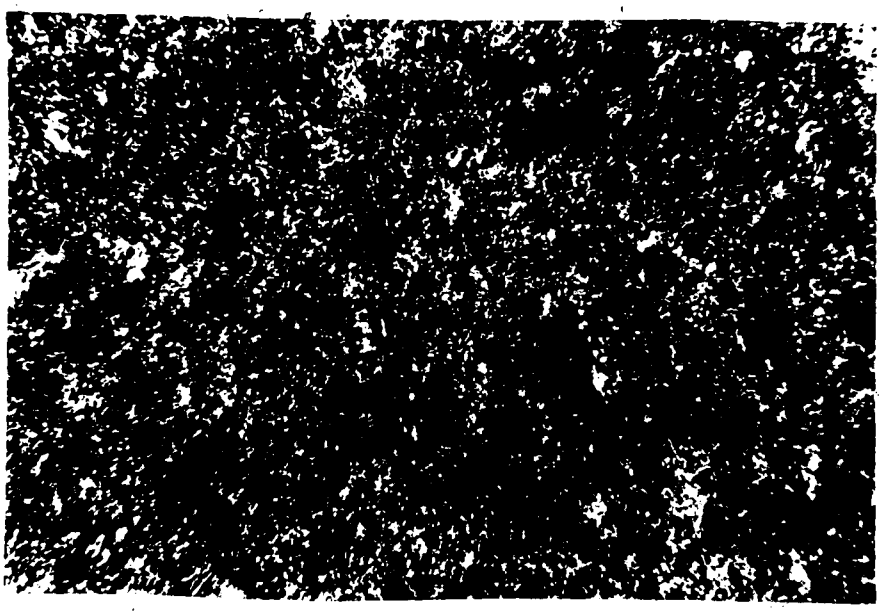

Z

Y

100μm

PLATE 19

BEDDING/CLEAVAGE

100μm

PLATE 20

Plate 21: Scanning electron micrograph of specimen 79-28. a)View of fractured surface normal to coincident bedding-cleavage planes. Note the predominance of flake edges and subparallelism of flakes.

b) View of bedding/cleavage plane, showing large proportion of basal planes.

a)

10μm

b)

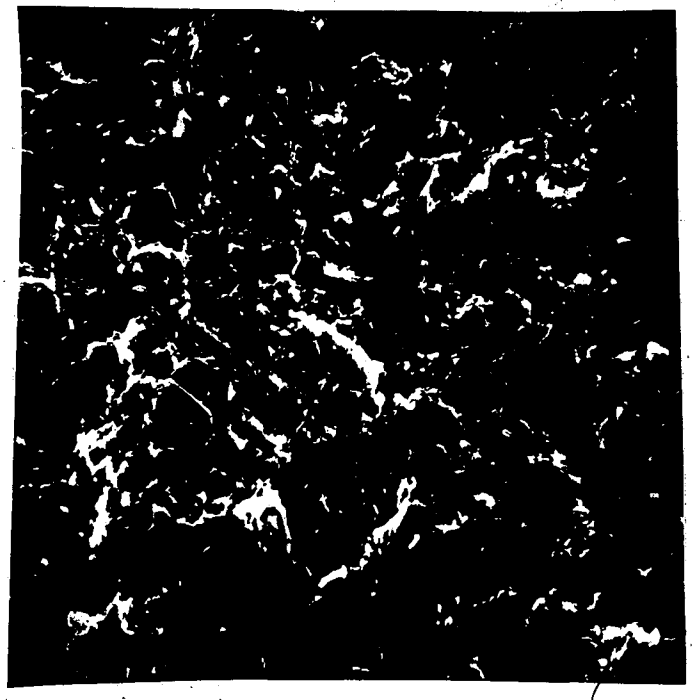

100μm

PLATE 21

Plate 22: Scanning electron micrograph of specimen 79-31, view normal to bedding and cleavage, stereo pair. a) is right, b) is left. Cleavage traverses view vertically; bedding trace is WNW. In this specimen, cleavage zone was apparently more cohesive than surrounding material, giving it higher relief on fracture surface; this relief accounts for relative brightness in the photographs. Note well defined parallelism of clays within folium.

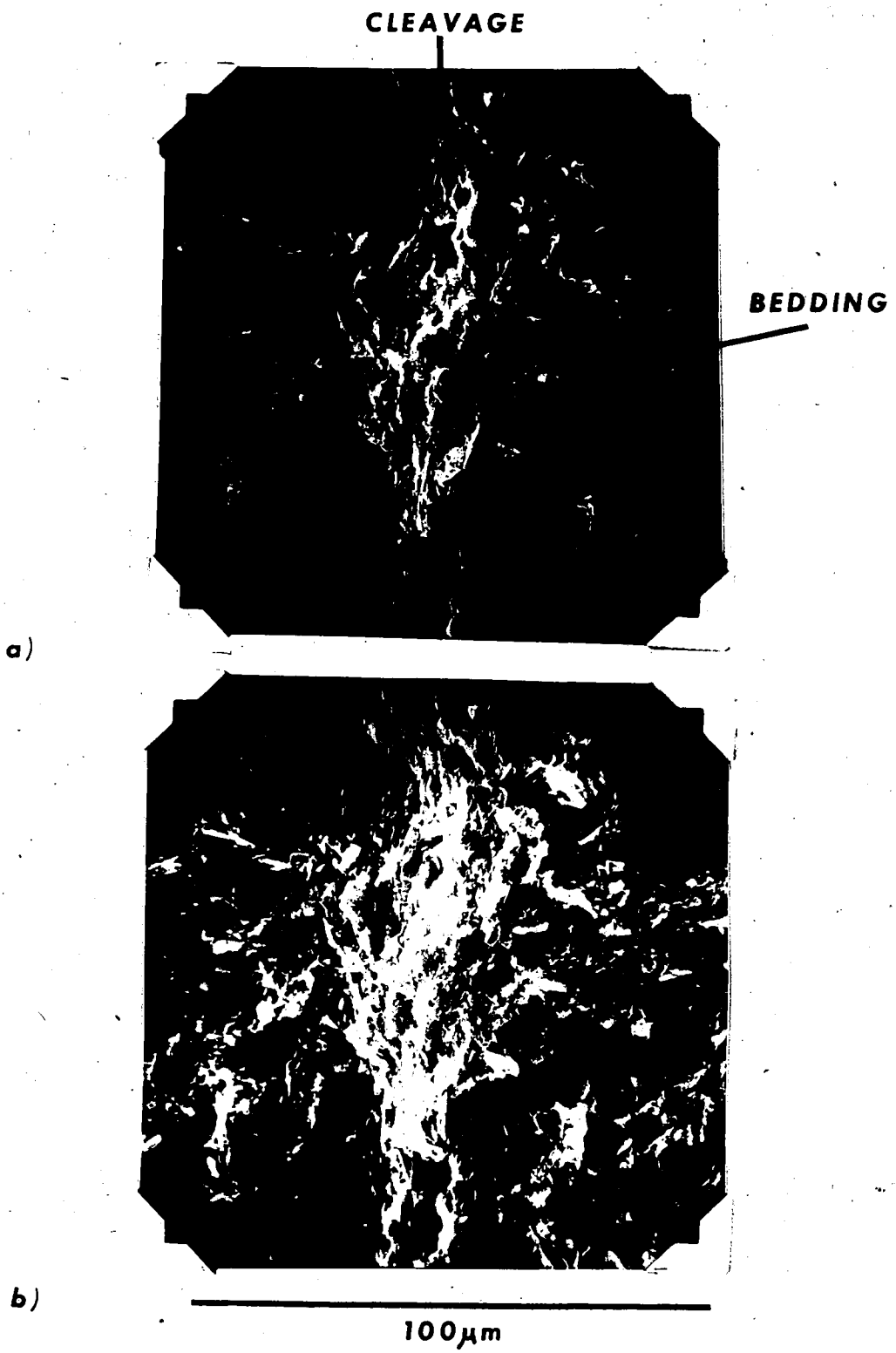

PLATE 22

Plate 23: Specimen 79-31; scanning electron micrograph, normal to bedding and cleavage. Note somewhat chaotic nature of cleavage zone; some clay flakes are apparent with orientations intermediate to those of bedding and cleavage.

PLATE 23

Plate 24: Scanning electron micrograph of specimen 79-31, view of bedding plane. Cleavage zone traverses east-west.

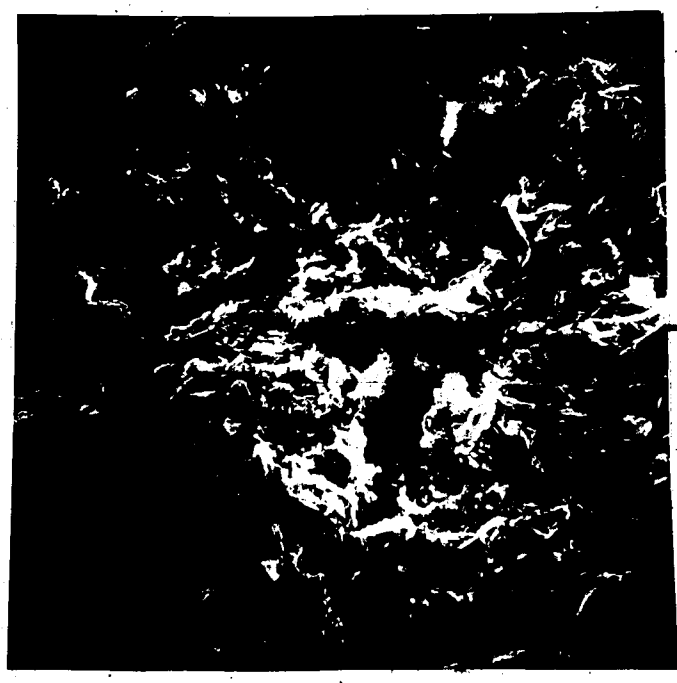

100μm

PLATE 24

Plate 25: Specimen 79-31, crossed nichols, gypsum plate. Same field as plates 30 and 31, rotated approximately 90° clockwise, with very high magnification. Cleavage runs NE-SW. Note chaotic nature of cleavage zone; larger micas are well oriented, but smaller clays are more random in attitude. Objective 95x oil immersion.

Plate 26: Specimen 79-31, crossed nichols, mica plate. Section normal to cleavage and bedding. Dark area is cleavage folium. Objective 50x.

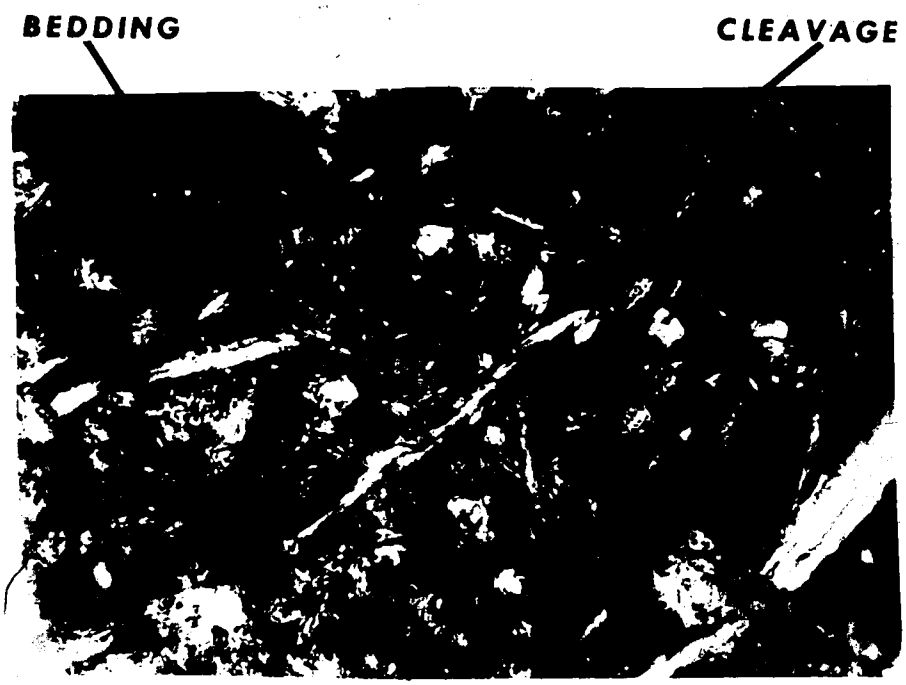

10μm

PLATE 25

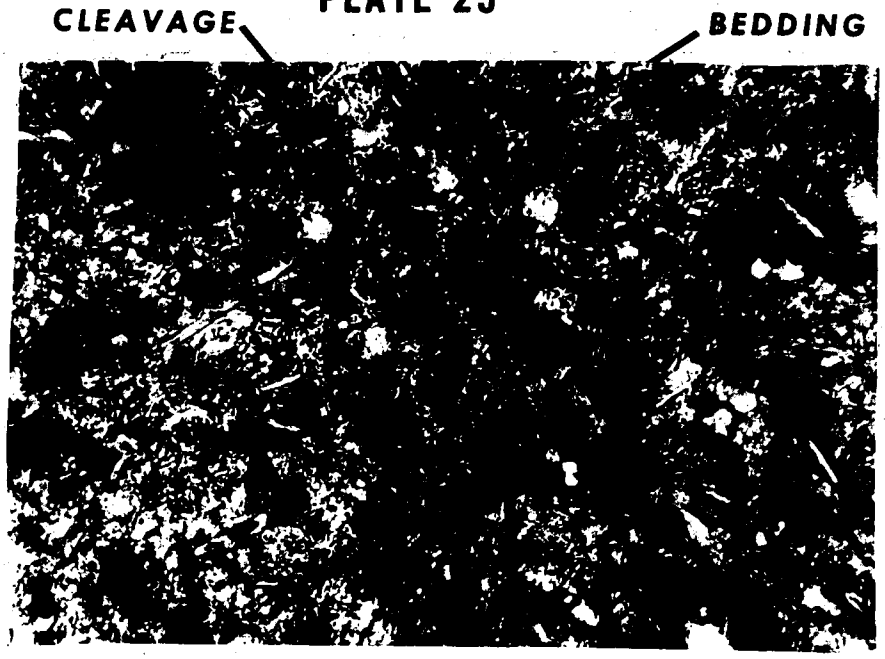

100μm

PLATE 26

Plate 27: Specimen 79-31, crossed nichols, mica plate. Section normal to both bedding and cleavage. Cleavage runs NW-SE; bedding (NE-SW) also apparent in this view. Objective 50x.

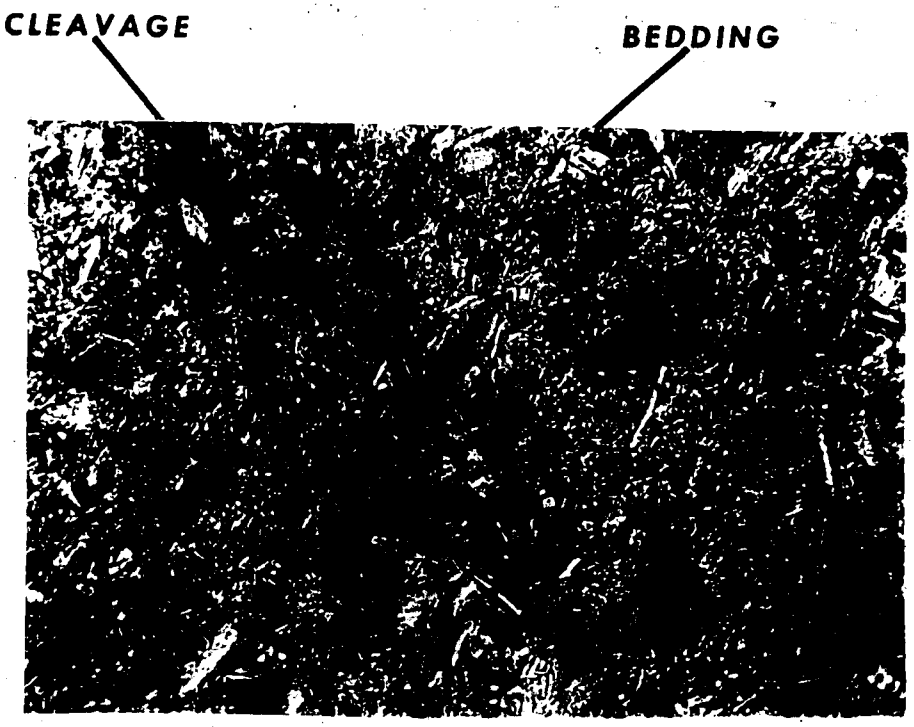

100μm

PLATE 27

Plate 28: Scanning electron micrograph of 79-31, view normal to bedding and cleavage. a) and b) same fields, magnification of b) twice that of a). Two cleavage folia are shown. Note subparallelism of clay flakes within the folia, and their high inclination to the trace of the bedding plane, which is apparent elsewhere in the field of view.

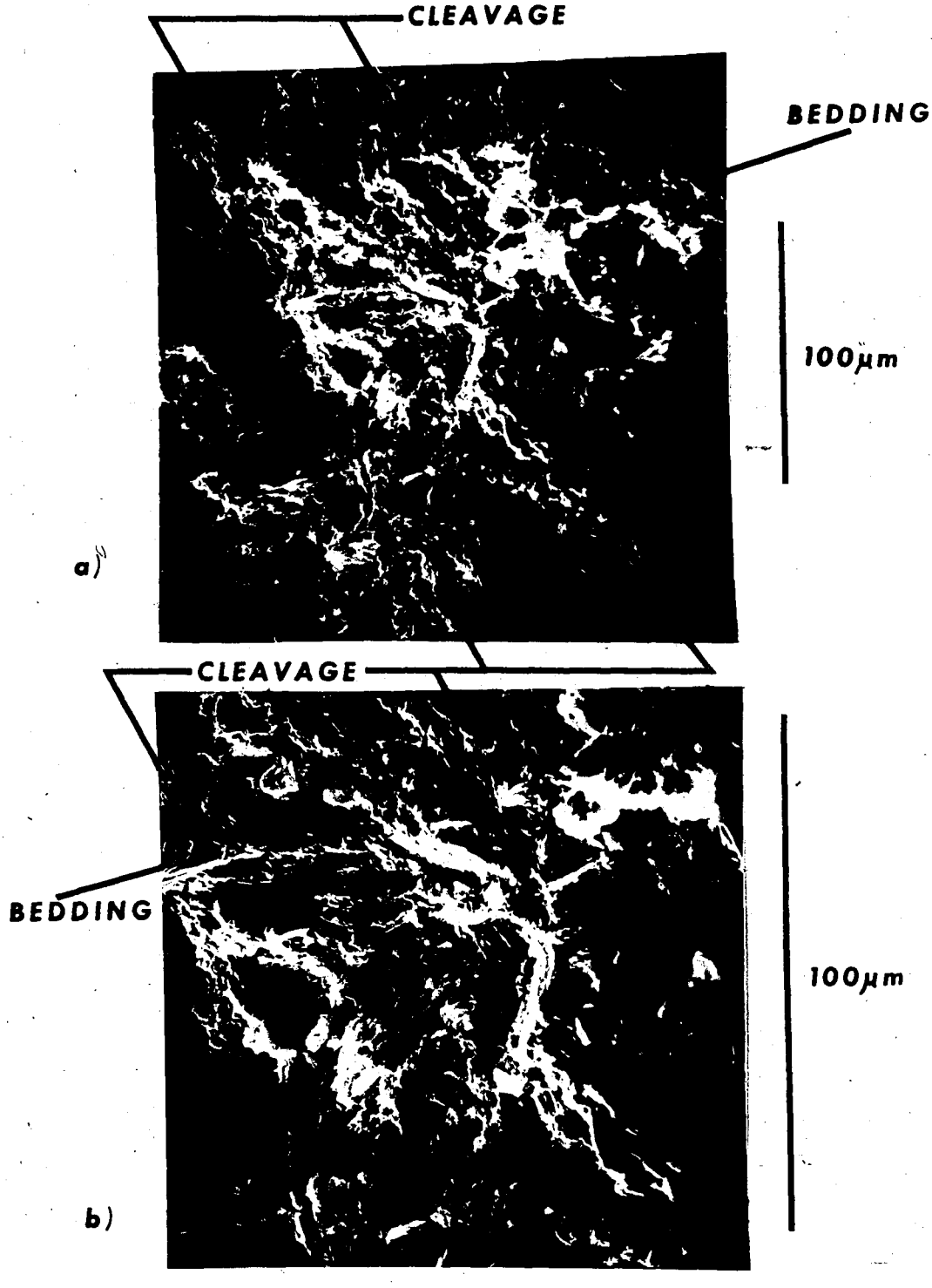

PLATE 28

Plate 29: Scanning electron micrograph of specimen 79-31. Same field in both a) and b), magnification of b) twice that of a). Cleavage trends from lower left to upper right; bedding is nearly horizontal. Along both edges of cleavage zone clay flakes can be seen with orientations intermediate to those of bedding and cleavage, suggesting upward flow of fluid within the cleavage zone.

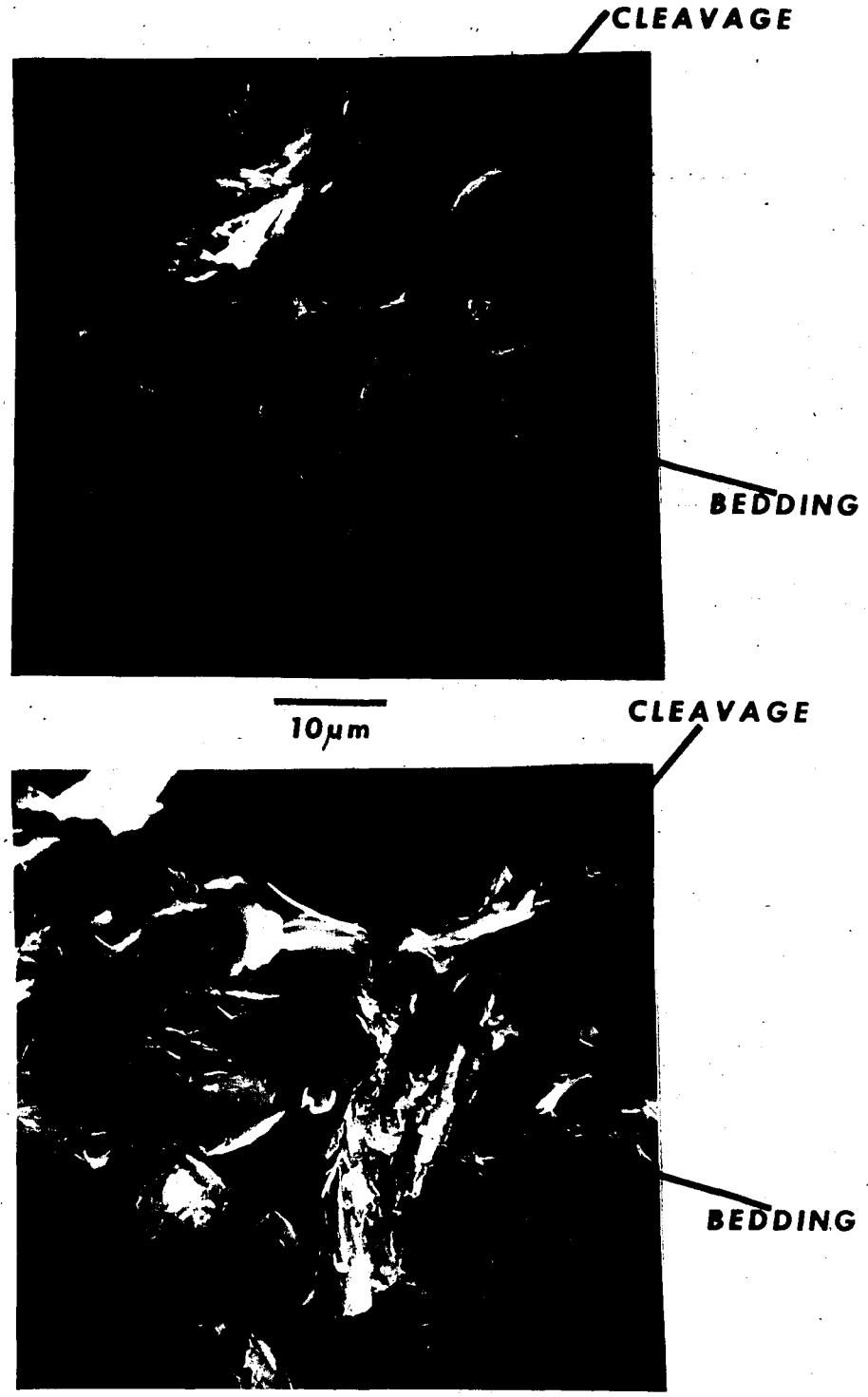

PLATE 29

Plate 30: Specimen 79-31, crossed nichols, mica plate. Section normal to bedding and cleavage. Cleavage folia trend NW-SE. One narrow folium visible in right quarter of view; another, much wider, anastamosing folium can be seen at left. Objective 10x.

Plate 31: Specimen 79-31, crossed nichols, mica plate; same field as plate 2, higher magnification. Objective 25x.

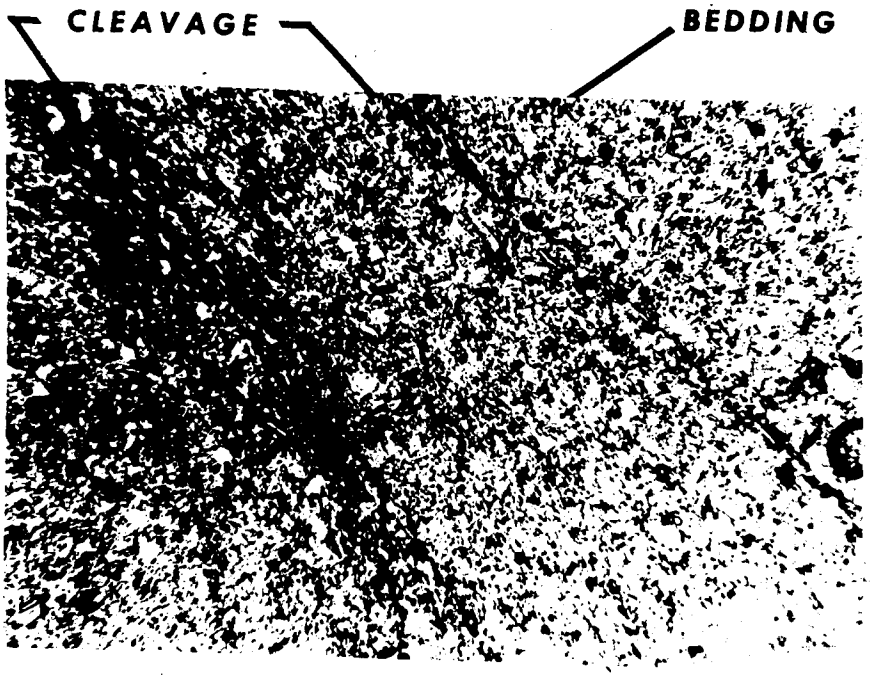

PLATE 30

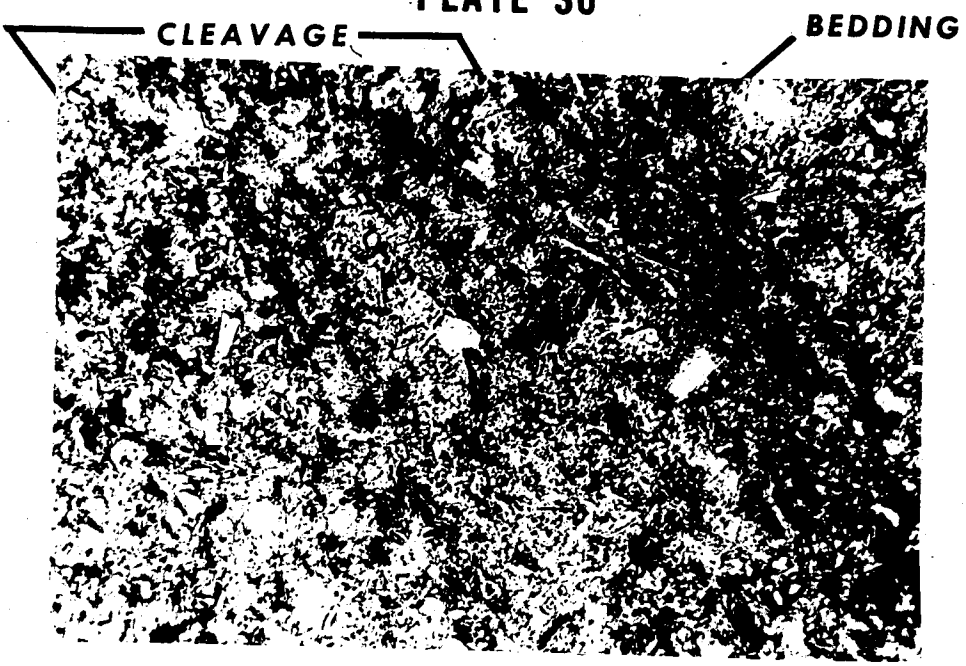

PLATE 31

Plate 32: Specimen 79-31; crossed nichols, mica plate. Section parallel to bedding, normal to cleavage. Cleavage is dark zone running NW-SE. Objective 10x.

Plate 33: Specimen 79-31; crossed nichols, mica plate. Section parallel to bedding, normal to cleavage. Cleavage is dark zone running NW-SE. Objective 25x.

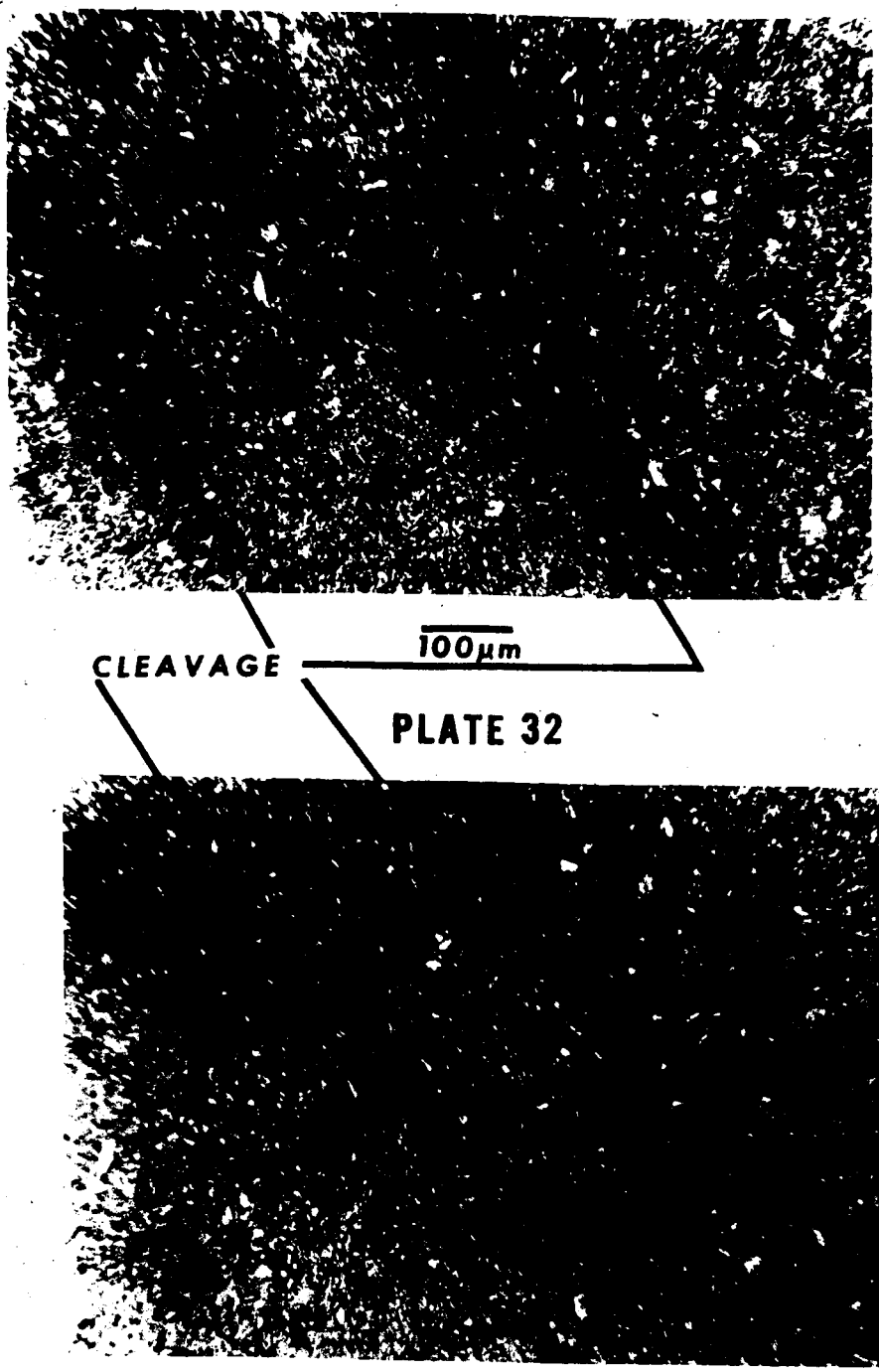

PLATE 32

100μm

PLATE 33

Plate 34: Specimen 79-31, crossed nichols, gypsum plate. Section normal to bedding and cleavage. This folium is larger than is typical, reaching a width of nearly 200 μm where it bifurcates. Dark and light bands parallel to bedding are an artifact of epoxy impregnation. Objective 3.5x.

Plate 35: Specimen 5-2, yz plane; crossed nichols, gypsum plate, red light. Preferred orientation, possibly resulting from horizontal compression, oriented nearly parallel to y axis, here rotated 45°. A few small shear zones are evident, with flakes nearly parallel to the z axis. Objective 10x.

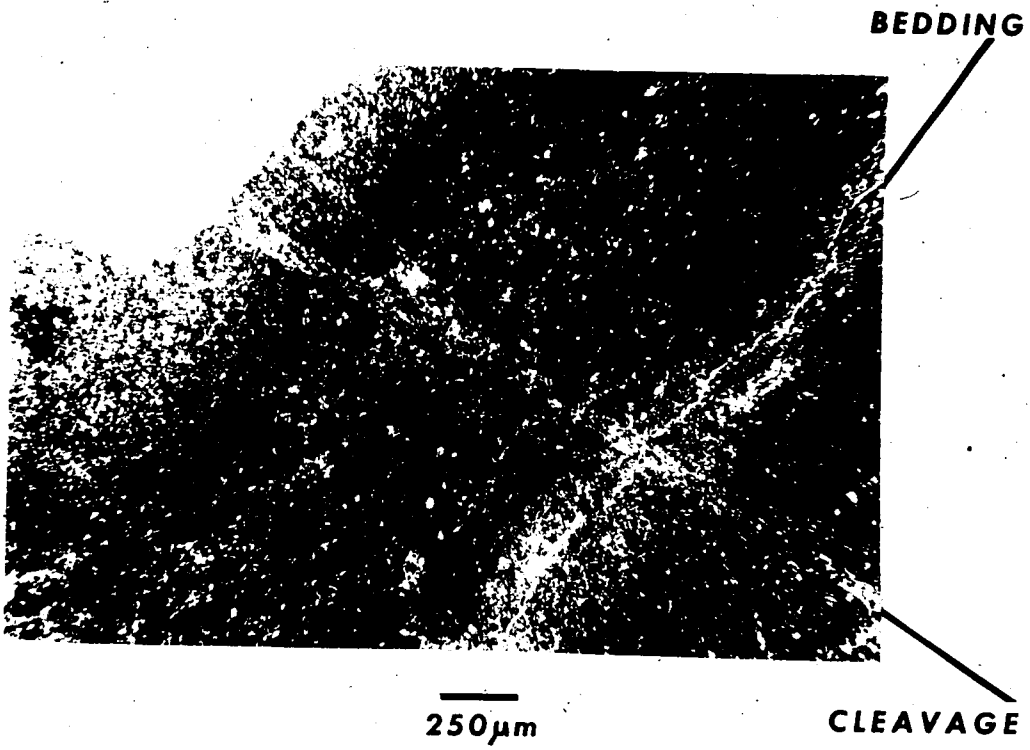

PLATE 34

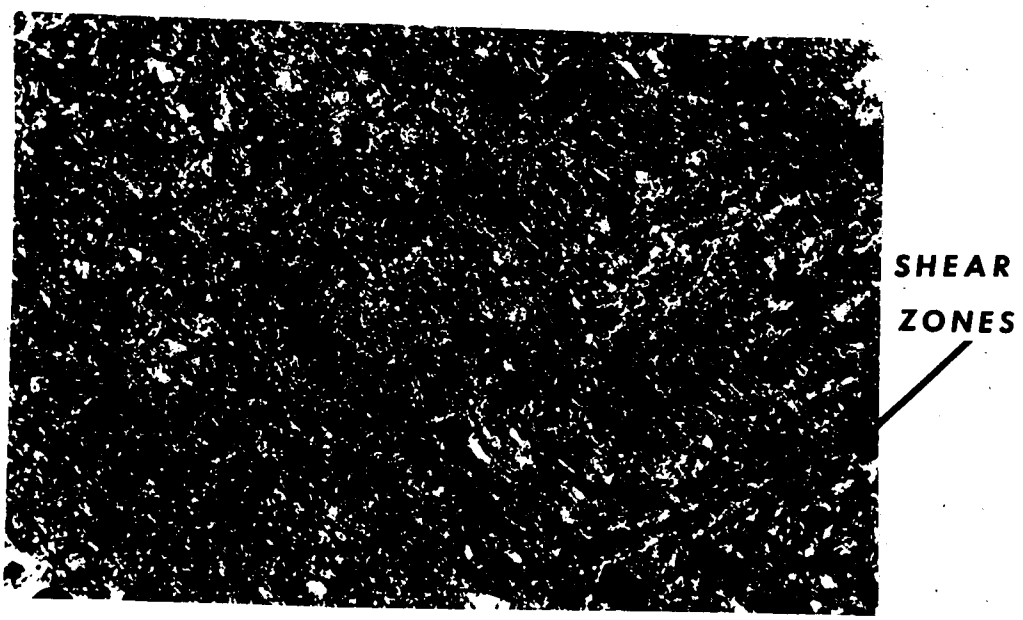

PLATE 35

Plate 36: Specimen 5-4, yz plane. Preferred orientation of unknown origin, tracing NW-SE. Objective 10x.

Plate 37: Specimen 5-4, xz plane; crossed nichols, gypsum plate, red light. Preferred orientation of unknown origin, tracing NW-SE. Objective 10x.

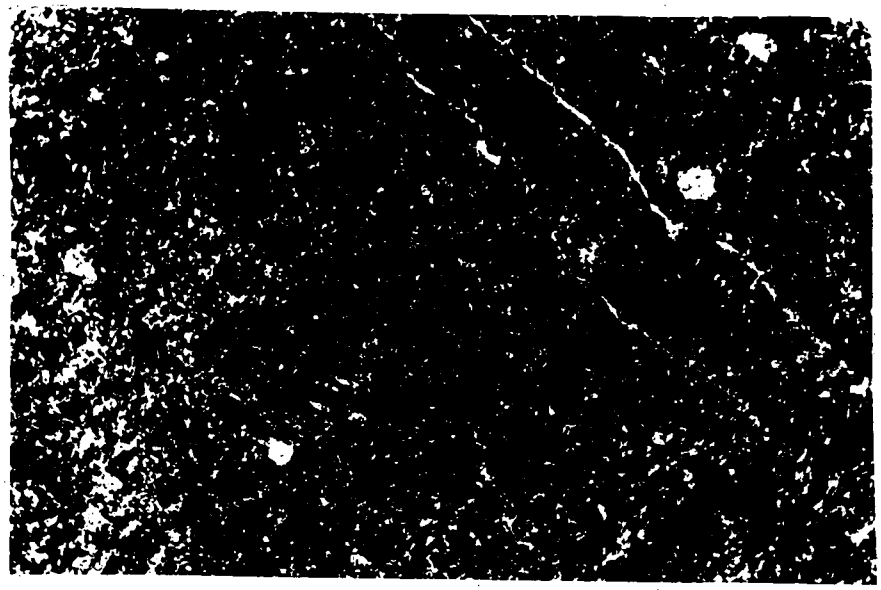

PLATE 36

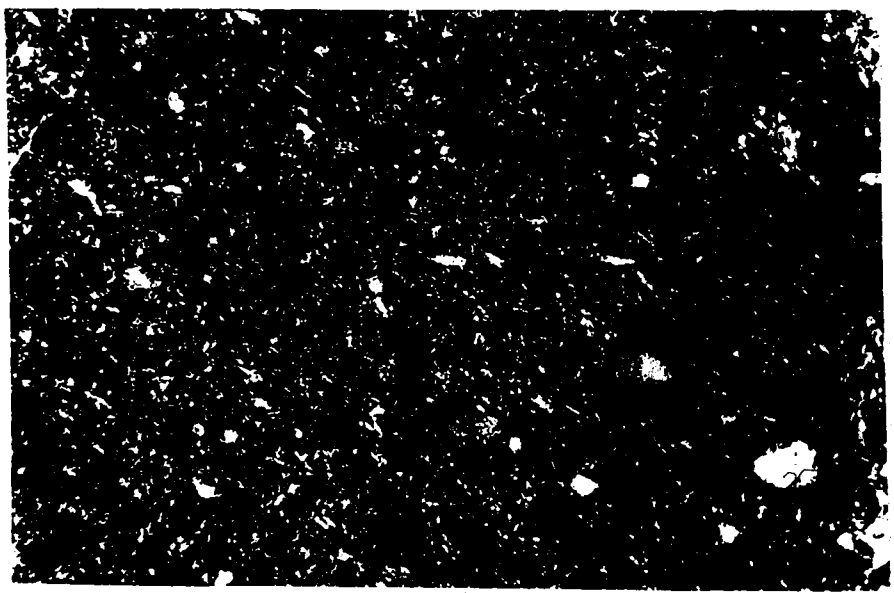

PLATE 37

Plate 38: Specimen 5-2, xz plane; crossed nichols, gypsum plate, red light. Large scale view of shear zones in plate 3. Objective 3.5x.

Plate 38: Specimen 5-2, xz plane; crossed nichols, gypsum plate, red light. Large scale view of shear zones in plate 3. Objective 3.5x.

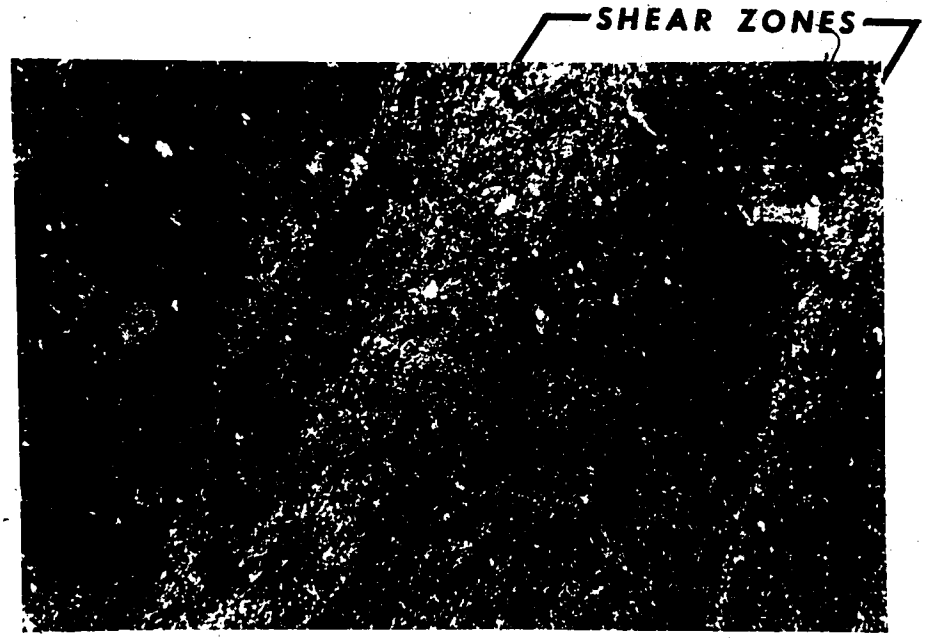

PLATE 38

Plate 39: Scanning electron micrograph of specimen 79-31; composite view normal to bedding and cleavage; trace of bedding, east-west; trace of cleavage, nearly north-south.

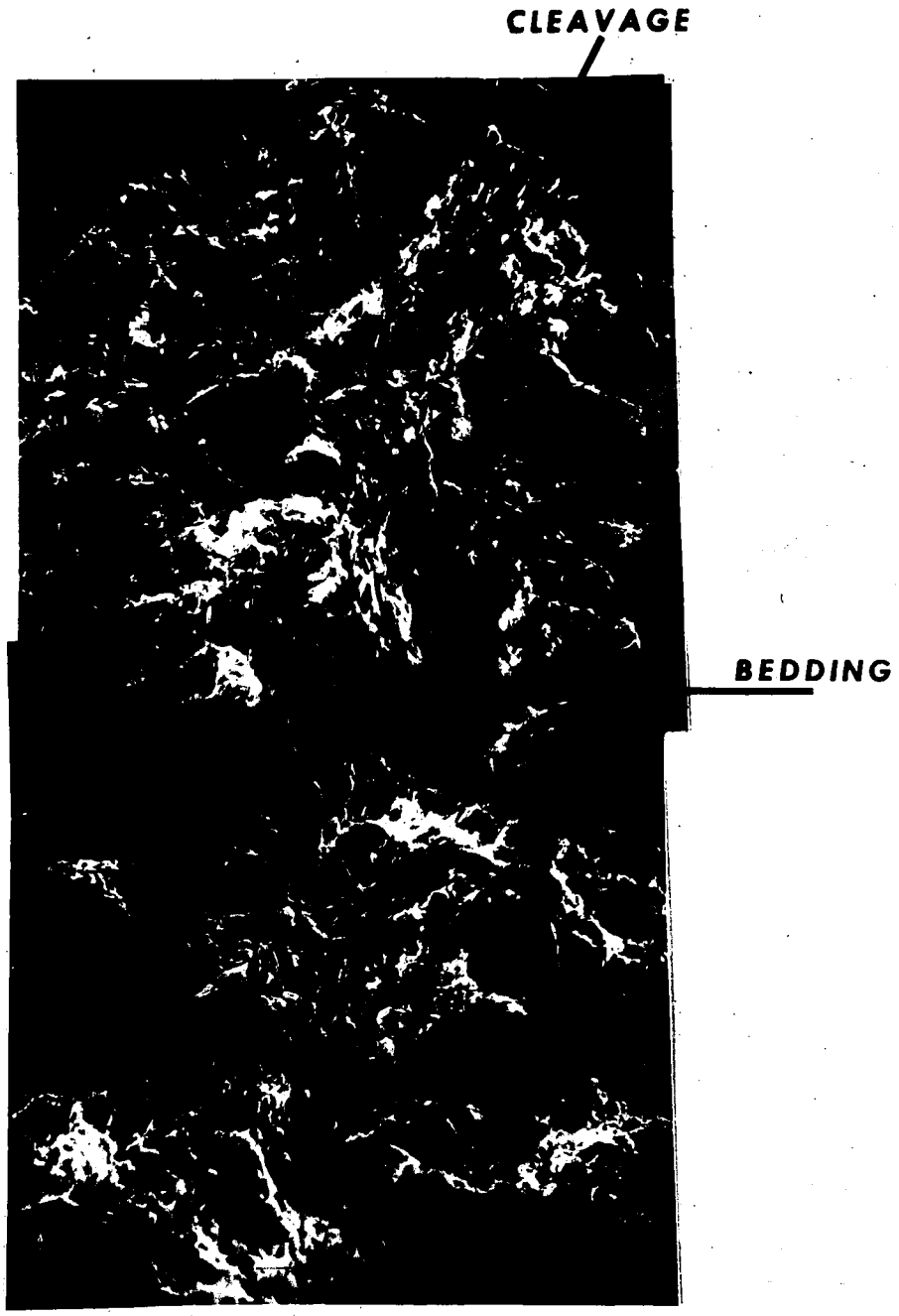

100μm

PLATE 39

Plate 40: Scanning electron micrograph of specimen 79-31, view of foliation surface. Note preponderance of basal planes. Bedding orientation is vertical, perpendicular to photographs. Same field in b) as in a), with twice the magnification.

a)

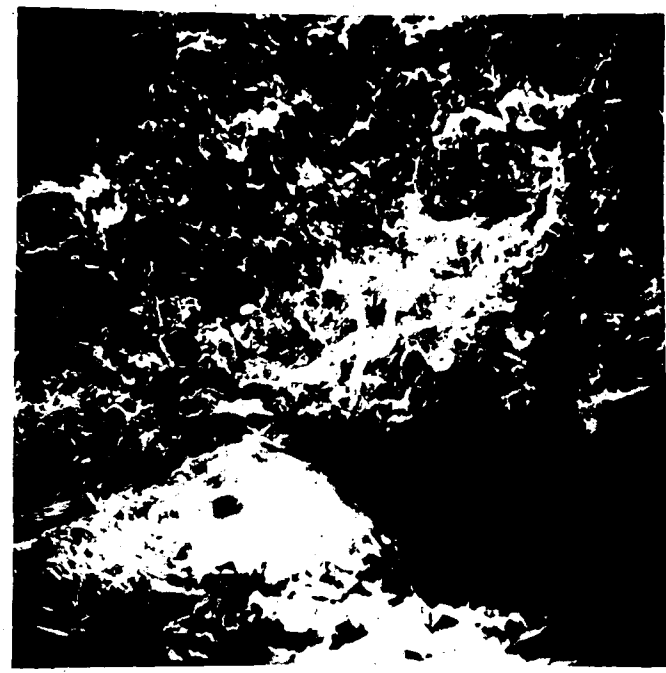

100μm

b)

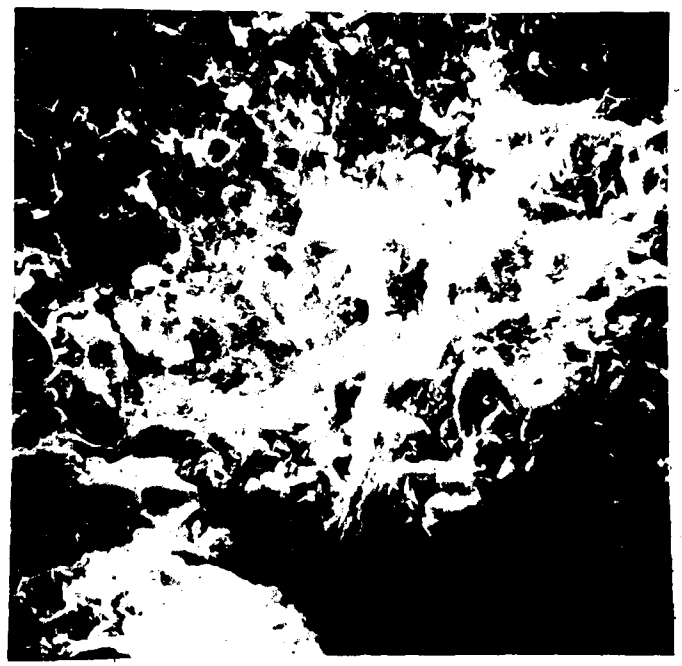

100μm

PLATE 40

Plate 41: Scanning electron micrograph of specimen 79-31, view of bedding poane, stereo pair. a) is right, b) is left. Cleavage zone traverses the photographs east-west. At this relatively low magnification, micas are more apparent than clays; stereo viewing reveals them to lie in a nearly vertical attitude. The surface was exposed by fracturing the specimen along bedding; the lower half of this area separated at a slightly higher bed than did the upper half, giving the cleavage plane the appearence of a step.

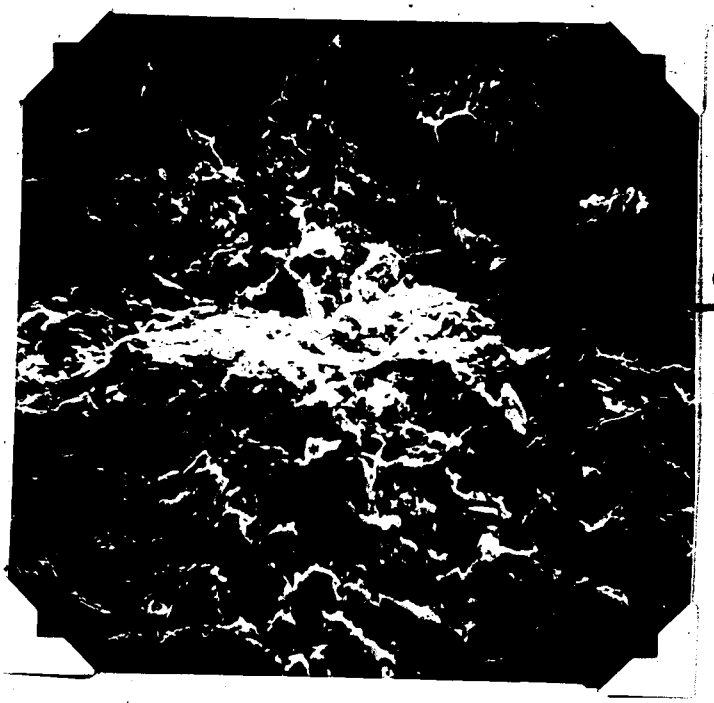

a)

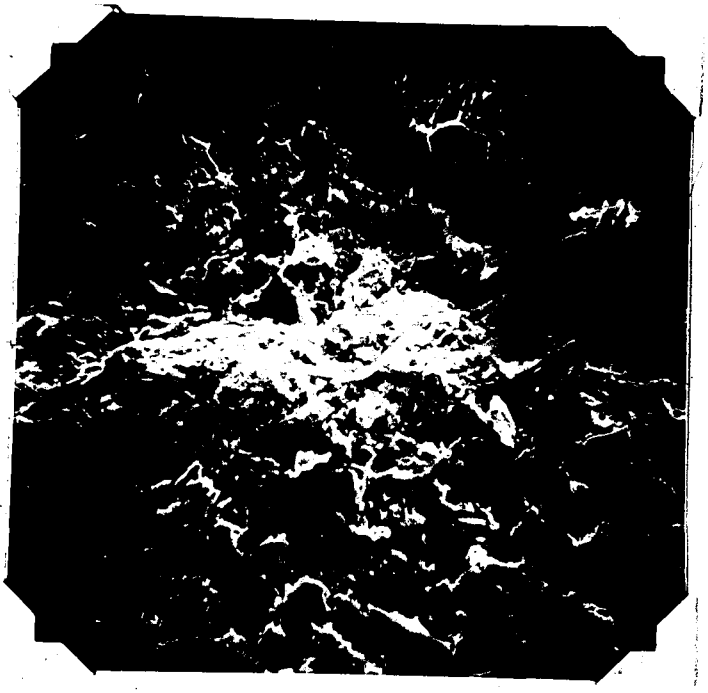

b)

100μm

PLATE 41

VITA

Peter L. Berglund was born in Philadelphia, Pennsylvania, on November 6, 1950 to Rev. John W. and Rosalind M. Berglund. He married M. Christine Walsh and has three children, Carrie, Timothy, and Brian. He received a BA in geology from Lafayette College in 1973 and completed course work for an MS in geology at Lehigh University in 1978. While at Lehigh he received a scholarship from the Society of Exploration Geophysicists and was employed as a research assistant in the Department of Geological Sciences. He is currently employed as a geophysicist by Amoco Production Company in Denver, Colorado.